https://doi.org/10.5194/egusphere-2025-5568
Preprint. Discussion started: 9 December 2025

Light-weight Observatory for sOuNdIng clouds and aeorSol, LOONIS: a balloon lifted platform for atmospheric aerosol research

Luis Valero[1], Konrad Kandler[1], Sina Jost[2], Holger Tost[2], Luca Katarina Eichhorn[2], Christian von Glahn[2], Harald Rott[2], Marilena Flory[1], Alexandre Baron[3,4], Kathie Smith[3,4], Troy Thornberry[4], and Ralf Weigel[2]

[1]Institute of Applied Geosciences, Technical University of Darmstadt, Darmstadt, 64287, Germany.
[2]Institute for Physics of the Atmosphere, Johannes Gutenberg University, Mainz, 55128, Germany
[3]Cooperative Institute for Research in Environmental Sciences (CIRES), University of Colorado, Boulder, CO, USA
[4]NOAA Chemical Sciences Laboratory, Boulder, CO, USA

Correspondence: Luis Valero (valerotuya@geo.tu-darmstadt.de)

Abstract. High-altitude aerosol research is crucial but faces significant cost and logistical hurdles that limit our ability to capture the highly variable vertical distribution of atmospheric trace substances. This paper introduces the Light-weight Observatory for sOuNdIng clouds and aerosol (LOONIS), a versatile, cost-effective, balloon-borne platform that provides an approach to address these challenges. LOONIS integrates a suite of lightweight instruments, such as optical particle counters, which provides real-time in situ detection of aerosol particle number and their microphysical properties, and impactors for collecting particles due to their inertia for subsequent offline physico-chemical analyses. Deployed during two measurement campaigns in Germany during August 2023 and June 2024, LOONIS provided insights into vertical aerosol distribution, capturing aerosol activation processes within saturated atmospheric layers.

The platform demonstrated enhanced accuracy of particle concentration data from the UCASS instrument through the integration of a Thermal Flow Sensor (TFS). The deployment and resulting dataset underscore LOONIS's capability as a tool for improving our understanding of atmospheric processes and potentially reducing the knowledge gap in atmospheric aerosol processes.

1 Introduction

Atmospheric aerosols and cloud droplets play a critical role in the Earth's climate system, influencing the radiation budget and hydrological cycle (Szopa et al., 2021). Accurate characterization of the particles' properties, such as particle size distribution (PSD) (O'Sullivan et al., 2020) and their physico-chemical properties (Pöschl et al., 2010) is one of the ways for reducing uncertainties in climate models (Seinfeld et al., 2016). It also improves our understanding of atmospheric processes like radiative forcing (Feingold et al., 2016) or cloud formation (Costa-Surós et al., 2020). However, obtaining in-situ measurements over the planetary boundary layer and above has historically presented significant logistical and financial challenges. Some methods, such as aircraft-based research campaigns, provide detailed microphysical characterization but are inherently expensive to deploy and operate (Rossi et al., 2022), which limits the temporal coverage of atmospheric soundings (Dubey et al., 2022). The substantial cost per flight hour for research aircraft restricts the feasibility of extensive studies (Li et al., 2025b).

https://doi.org/10.5194/egusphere-2025-5568
Preprint. Discussion started: 9 December 2025

Balloon-borne sounding systems offer a flexible and cost-effective alternative for acquiring vertically resolved atmospheric data (Joly et al., 2016). Weather balloons, capable of reaching the Upper Troposphere/Lower Stratosphere (UTLS) (Golden et al., 1986), provide a platform for in-situ measurements with significantly reduced operational costs compared to aircraft (Rossi et al., 2022) or satellite deployment missions (Li et al., 2025b). While aircraft-based measurements provide horizontal transects across potentially vast regions (Pikridas et al., 2019), their rapid passage can limit the characterization of vertical structures. Conversely, the slow ascent of a balloon provides a detailed vertical profile, enabling the resolution of fine-scale features within dynamic systems that can extend throughout the troposphere, such as desert dust intrusion (Papayannis et al., 2008), developing clouds (Evan et al., 2020) or volcanic dust plumes (Kloss et al., 2022). Furthermore, the limited lifespan of atmospheric events means the window of opportunity is short, from hours (Piper et al., 2019) to a few days (Varga, 2020) and balloon platforms offer significant flexibility in payload configuration and deployment time. Unlike the fixed instrumentation of satellites or the long planning of an aircraft campaign (Li et al., 2025b), balloon payloads can be adapted and prepared for immediate use. This modularity enables researchers to integrate various sensors and measurement techniques on a single sounding, allowing for more targeted data acquisition for a range of atmospheric parameters. For example, different types of optical particle counters (OPCs) can be combined to cover a broader size range or target specific aerosol diameter sizes (Kezoudi et al., 2021).

Since the payload for a balloon is limited by physical and legal constraints, the most essential measurements are strategically chosen to fit scientific objectives. In the current approach we selected aerosol size distribution and aerosol composition as parameters of greatest interest. For balloon-borne use, the most suitable means of size distributions measurements appear to be optical particle counters. Aerosol concentrations are typically low for this region, therefore nozzle impactors were chosen for aerosol collection.

OPCs utilize the principle of light scattering to determine the optical size of individual particles. They also offer high temporal resolution and have been widely employed for in-situ aerosol measurements on both stationary (Dupont et al., 2025) and mobile platforms (Moormann et al., 2025), making them a cost-effective solution for aerosol research. The development of lightweight and cost-effective sensors has enabled measurements on a new generation of small unmanned aircraft systems (UASs) (Bates et al., 2013; Altstädter et al., 2015) and balloon platforms (Kezoudi et al., 2021). OPCs are suitable for most in-situ aerosol experiments (Mamali et al., 2018) as they provide information on particle number concentration and size distributions from the accumulation to the coarse mode. Different aerosol size modes exhibit distinct properties that interact with tropospheric air masses (Li et al., 2025a), particularly their ability to act as cloud condensation nuclei (CCN) (Kasparoglu et al., 2024). For this article, we focus on the larger accumulation (0.1 μm - 2.5 μm) and coarse (> 2.5 μm) modes, as particles in these ranges are more likely to activate into cloud droplets under typical atmospheric supersaturation conditions (Seinfeld and Pandis, 2016; Pöhlker et al., 2023).

Measuring a broad spectrum of aerosol sizes, from the nucleation to the coarse mode, is essential for understanding their impacts on climate and atmospheric processes (Carslaw et al., 2010). However, obtaining accurate size measurements requires careful consideration of environmental factors. For instance, hygroscopic growth can significantly increase the apparent particle size in humid air, a phenomenon observed in most atmospheric aerosols, including mineral dust (Swietlicki et al., 2008; Koehler

https://doi.org/10.5194/egusphere-2025-5568
Preprint. Discussion started: 9 December 2025

et al., 2009). Consequently, integrating different sensing technologies within a single measurement platform allows for more detailed and comprehensive investigations of aerosol properties (Kezoudi et al., 2021).

While OPCs are effective for characterizing aerosol PSDs, a more comprehensive understanding requires collecting particles for subsequent chemical analysis. Impactors are a useful tool for this task, as they collect particles based on their inertia, efficiently capturing larger particles for off-line characterization of their physico-chemical properties (Kandler et al., 2009). For this detailed single-particle analysis, scanning electron microscopy (SEM) coupled with energy-dispersive X-ray spectrometry (EDX) is an effective combination. This method involves focusing an electron beam onto a collected particle, which generates several key signals. Secondary electrons (SE) produce high-resolution images of the particle's surface topography, while backscattered electrons (BSE) reveal contrasts based on the material's atomic number (Johnson, 1996). Simultaneously, the characteristic X-rays emitted from the sample are analyzed by EDX to determine the particle's surface elemental composition. Together, these techniques provide integrated morphological and chemical information on a particle-by-particle basis.

Tropospheric trace matter over different vertical air layers can be effectively characterized by combining two complementary instruments, OPCs and impactors, with offline analyses using SEM and EDX. This paper describes the balloon-borne Light-weight Observatory for sOuNdIng clouds and aeorSol (LOONIS), its design and laboratory development for tropospheric aerosol research and its application during the transport of aerosols and precursors from the planetary boundary layer into the UTLS- BrIdging Surface emissions, Transport and UTLS Matter (BISTUM) field campaign. This integrated approach provides a more detailed understanding of aerosol properties in the vertical column than either measurement technique could achieve alone.

2 Light-weight Observatory for sOuNdIng clouds and aeorSol (LOONIS)

2.1 Overview of LOONIS

The balloon-borne measurement platform (Fig. 1) is designed for atmospheric research, carrying a set of instruments to gather relevant atmospheric data. The platform that can be divided into three key areas: a) technical parts comprising the core electronics and power systems b) the operation encompassing data acquisition, transmission and structural elements (see table 1). c) instruments for environmental measurements (see table 2).

The platform utilizes a single board computer (SBC) as its central controller, interfacing with various sensors to gather data, which is subsequently processed by the SBC, and then selected data packages are transmitted continuously each second to a ground station for live monitoring and post-flight analysis.

The system is powered by two independent sources to ensure continuous operation. Physically, the payload is mounted on a carbon fiber structure with two polystyrene boxes. One box is dedicated to the Vaisala RS41 radiosonde model SGP and the electrochemical concentration cell (ECC) for ozone (from Environmental Science Corporation). The second box holds the pumps, SBC, support sensors and main battery. The payload is connected to the balloon via a suspension rope. This rope attaches to the upper end of the aluminum rod. Since the payload is modular keeping the payload mass perfectly centered is not possible. Therefore the payload has a comparatively long (0.67 m) pole attached to the structure, mitigating an imbalance.

https://doi.org/10.5194/egusphere-2025-5568
Preprint. Discussion started: 9 December 2025

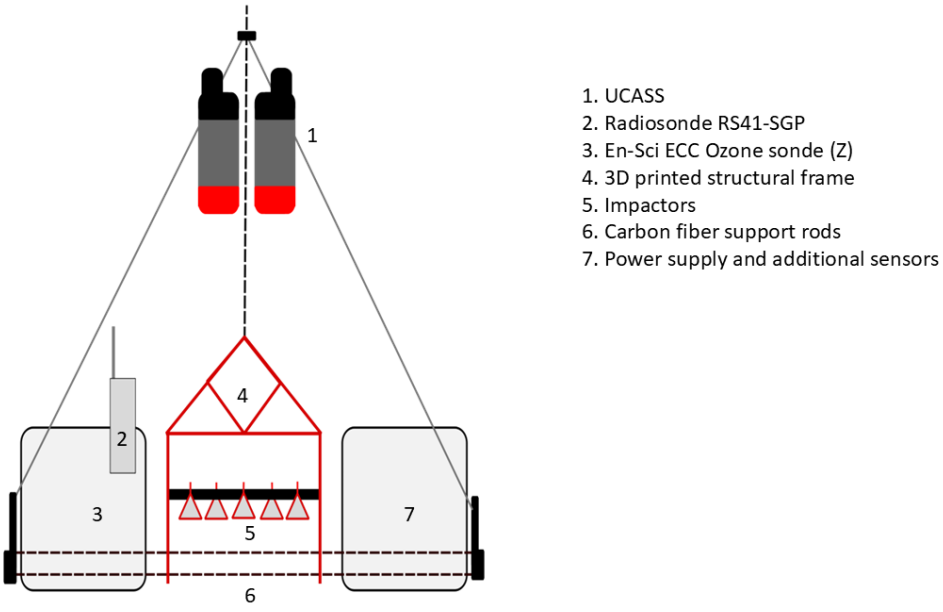

Figure 1. Schematic of the Light-weight Observatory for sOuNdIng clouds and aeorSol (LOONIS) payload. The configuration shows the primary instruments for in-situ atmospheric measurements. Aerosol optical properties are measured by two Universal Cloud and Aerosol Sounding System (UCASS) optical particle counters (1), while ozone and meteorological data are provided by an En-Sci ECC Ozone sonde (3) and a Vaisala RS41-SGP radiosonde (2), respectively. A set of dual-stage impactors (5) is integrated for the physical collection of particles for later analysis. These components are housed within a central 3D-printed structural frame (4) and supported by carbon fiber rods (6), with the power supply and auxiliary sensors located in a separate module (7).

Base payload parts	**Description**	**Optional**	**Weight**
Raspberry Pi Model 3B+	Manages sampling, data collection and transmissions	✗	50 g
4 x Battery (5200 mAh 10 A)	Supply power to the payload´s different parts	✗	300 g
Camera (IMX219)	Records footage	✓	85 g
Chassis	3-D-printed frame structure	✗	650 g
Boxes (24x16x16 cm)	Polystyrene to isolate electronics	✗	120 g
Support rods (80 cm)	Carbon fiber rods that preserve the position of the boxes	✗	180 g
		Base mass	**1385 g**

Table 1. LOONIS base payload and supporting elements. Base mass and total mass may vary for different units due to different amount of tape, screws, cable ties and other assembly materials used.

https://doi.org/10.5194/egusphere-2025-5568
Preprint. Discussion started: 9 December 2025

Sensor	Variable	Optional	Sampling time	Power consumption	Weight
RS41-SGP Vaisala Radiosonde	Temperature, relative humidity, pressure, GPS location	✗	1 s	9 W	96 g
UCASS (Universal Cloud and Aerosol Sounding System)	Particle size distribution	✗	0.5 s	3 W	200 g
FLW-122 Thermal flow sensor	Flow speed (inside UCASS)	✓	0.25 s	≈ 15 mW	2 g
POPS (Portable Optical Particle Spectrometer)	Particle size distribution	✓	1 s	7 W	800 g
Dual stage impactors + Pumps	Particle collection	✗	1200 s	2.4 W	300 g
Alphasense CO-B4	CO Concentration	✓	0.25 s	≈ 15 mW	12 g
ECC ozonesonde	O_3 Concentration	✗	1 s	12 W	450 g
BMP280	Pressure, temperature	✗	1 s	≈ 15 mW	1 g
MPU6050	6-axis acceleration	✓	0.05 s	≈ 15 mW	1 g
Solar sensor	Light intensity	✓	0.25 s	≈ 15 mW	3 g
NEO-6M	GPS location	✗	1 s	≈ 15 mW	10 g
INA219	Voltage, intensity		1 s	≈ 15 mW	12 g
				Base mass	**1887 g**

Table 2. LOONIS instruments and supporting elements. Base mass and total mass may vary for different units due to different amount of tape, screws, cable ties and other assembly materials used.

2.2 Balloon Instrumentation Payload

The maximum weight, excluding balloon, parachute and ropes is limited to 4 kg due to legal restrictions (European Commission, 2012), thus making weight a critical factor in the instrumentation choice. The chosen variables to collect are: particle number concentration, CO ppb, O_3 partial pressure, temperature, humidity and GPS position. The dual-stage impactor is used to collect particles for offline analysis, which in turn provides morphology and chemical composition. The Portable Optical Particle Spectrometer (POPS) (Gao et al., 2016) and the Universal Cloud and Aerosol Sounding System (UCASS) (Smith et al., 2019) are well-suited balloon-borne OPCs platforms that have been used in vertical soundings (Kezoudi et al., 2021; Vandergrift et al., 2024). These instruments provide a reliable means of obtaining measurements for different-sized aerosols during ascent.

2.2.1 UCASS

The Universal Cloud and Aerosol Sounding System (UCASS) is an optical particle spectrometer designed for in-situ measurements of aerosol and cloud particles from balloon soundings and small UASs (Smith et al., 2019; Girdwood, 2022; Kezoudi

https://doi.org/10.5194/egusphere-2025-5568
Preprint. Discussion started: 9 December 2025

et al., 2021). UCASS uses a diode laser beam through a defined sample area. When particles pass through the area, they cause the light to scatter and a detector measures the intensity of this scattered light, which is correlated to the particle's size. UCASS units are individually calibrated using a pitot tube (Girdwood, 2022) and can be adjusted to target different diameter ranges (Girdwood et al., 2025). Specifically, the instrument's electronics analyze the intensity of the light scattered by each particle to sort it into one of 16 discrete size bins.

The UCASS instrument is a tool used for the in-situ characterization of atmospheric aerosols, with its utility for providing high-resolution vertical profiles demonstrated in studies of Saharan dust over Cyprus: One such study (Kezoudi et al., 2021) used the instrument to characterize a Saharan dust layer (refractive index of 1.52), detecting dust particles (0.4-14.0 μm) with peak concentrations up to 50 particles per cm^3 . The findings showed reasonable agreement with aircraft data and highlighted the value of UCASS vertical profiles compared to remote sensing, though it was noted that UCASS-derived extinction was overestimated at high concentrations (> 25 particles per cm^3) (Kezoudi et al., 2021). In another application, the UCASS was used on a UAV as a reference sensor during a Cyprus dust event, reinforcing its use for validation (Schön et al., 2024). This work involved profiling a dust layer between 1500 and 2800 m with peak concentrations up to 35 particles per cm^3 (Schön et al., 2024).

UCASS does not feature any detector for the true air flow velocity through the open-path instrument. As a result, it needs to rely on the ascent rate or another external measurement (Smith et al., 2019). Instrument inclination or local flow disturbances therefore might lead to errors in concentration. To address this issue, a flow sensor was added to the system to directly measure flow speed (Jost et al., 2025). This allows for a more accurate calculation of the volume flow rate, improving upon methods that rely only on GPS ascent rates (Smith et al., 2019). This addition showed that the internal flow can deviate from the GPS-based ascent rate, typically by 10-30%, with peaks of up to 45% observed during soundings (Jost et al., 2025). The applicability of this specific thermal flow sensor was demonstrated up to an altitude of 7.5 km, a limit determined by ambient temperatures falling below the sensor's specified operational range.

To screen for faulty units prior to launch during both intense operation periods, we tested UCASS instruments using monodispersed particles of known sizes; 30 μm lycopodium powder (Sigma-Aldrich, 2025a), 1 μm and 10 μm monodisperse silica beads (Sigma-Aldrich, 2025c, b). After placing the UCASS in a small 12V fan powered wind tunnel, particles were manually dispersed into the flow. The UCASS categorizes each particle into several bins (in terms of diameter size) according to the intensity of its light-scattering signal. During these tests, the instrument performance was evaluated using the detection at the correspondent bin. For each flight, two units were deployed to measure distinct particle size ranges. One unit operated in droplet mode (UCASS_D), targeting larger particles, while the second operated in aerosol mode (UCASS_A), targeting smaller particles. As configured for the instruments in this study, the upper and lower limits are 0.3-32.5 μm for UCASSa and 9-51.5 μm UCASSd. The complete size range for all bins are detailed in the supplement (tables S2 and S3).

Between the 2023 and 2024 campaigns, UCASS units were recalibrated to verify optical alignment following mechanical impact during landing (Girdwood et al., 2025). Fixed fibres of carbon, tungsten, and glass were introduced to the sample volume, and the resulting scattering signals were validated against Generalised Lorenz-Mie Theory simulations to confirm the linear calibration coefficients.

https://doi.org/10.5194/egusphere-2025-5568
Preprint. Discussion started: 9 December 2025

2.2.2 POPS

The Portable Optical Particle Spectrometer (POPS) is a lightweight (800g), low-powered (5W) optical particle counter that measures aerosol number concentration and size for diameters between 140 – 2500 nm (Gao et al., 2016). Individual particles are detected as they pass through a 405 nm laser diode beam and the resulting amount of scattered light is related to their size following Mie theory, assuming a bulk index of refraction. In this study, we used n = 1.55 + 0.002i for layers impacted by dust transport and n = 1.45 + 0.00i otherwise. We used a 36 particle diameter size bins scheme and the pre-deployment calibration protocol using nebulized 508 nm polystyrene latex spheres (PSL) solution all described in (Todt et al., 2023). POPS applicability has already been shown in UAVs (Hagen Telg and Gao, 2017) and balloon borne payloads (Asher et al., 2024). The upper and lower limits are 0.14-2.5 μm for POPS and the complete size range is detailed in the supplement (Table S4).

2.2.3 Impactors

The impactor rack comprises a set of five dual-stage impactors (Fig. 1). These MINI dual-stage impactors are designed to collect aerosol particles by inertial impaction onto transmission electron microscopy (TEM) grids for subsequent analysis (Kandler et al., 2007b; Ebert et al., 2016). Laboratory calibrations using a Gilibrator 2 (Sensidyne, LP, 2020) showed that the total flow, limited by a critical orifice, measured 8.3 cm^3/s at standard conditions.

To control the air flow, each impactor is equipped with a dedicated miniature pump (Parker Hannifin Corporation, 2020). These pumps are activated sequentially based on ambient pressure measured during the ascent. Once triggered, each system operates for 20 minutes, drawing ambient air through a funnel inlet facing downwards. However, as the impactors remain open during the balloon's descent, the samples are susceptible to contamination from different altitudes.

The impactors are constructed to sample two size fractions with approximate size ranges divided approximately at 1 μm particle diameter. The lower limit is defined by a less steep efficiency curve and ranges from 30 nm to 150 nm approximately. The upper limit is constrained mainly by counting statistics and is in the range 5 - 10 μm. The housings of the impactors were 3D-printed from an epoxy-based resin while their orifices and substrate holders were produced from aluminum. The housing was exposed to temperatures down to -70°C for 24 hours, afterwards inspected for leaks; concluding that the external casting will endure harsh atmospheric conditions, protecting the TEM grid. Each flight usually delivers 10 samples on TEM grids, which serve as a standard sampling substrate, owing to the two-stage design. To minimize contamination the TEM grids are prepared and inserted into the impactor housing whilst in a clean environment. The housing is sealed until just before flight. After the sample has been collected the housing is resealed and the TEM grids are not removed until the impactor housing is returned to the clean environment.

2.2.4 Trace gases

The ECC Ozonesonde (EN-SCI, 2019) is a commercially available and widely used (Smit et al., 2024) electrochemical sensor designed for quantifying ozone (O_3) concentrations in air. A pump actively draws ambient air into the sensor's cathode

https://doi.org/10.5194/egusphere-2025-5568
Preprint. Discussion started: 9 December 2025

chamber, which contains a potassium iodide (KI) solution at 0.5%. In the solution, the reaction creates a measurable electrical current in the electrolyte of the sensor cell.

The strength of this electrical current is directly proportional to the amount of ozone present in the air sample. This measurement, combined with the air sampling rate and temperature, allows for the calculation of the ozone concentration, which is expressed in parts per billion by volume (ppbv).

The Alphasense CO-B4 (Alphasense, 2021) is a commercially available electrochemical sensor designed for quantifying carbon monoxide (CO) mixing ratio in air. CO gas diffuses into the sensor and undergoes an electrochemical reaction at the working electrode (WE), generating a current proportional to the CO concentration. The auxiliary electrode (AE) measures temperature and background current, enabling correction of WE voltage using one of the manufacturer-provided methods. The sensor features sensitivities in the range of 420-650 nA per ppm with a response time of 30 seconds (Alphasense, 2021) . The device's performance is characterized across a temperature range of -40°C to 85°C (Alphasense, 2021) and is influenced by temperature, humidity and pressure as well as cross sensitivity to other gases (Alphasense, 2019; Kim et al., 2018).

2.3 Payload components

For flight, the entire payload assembly is attached beneath an unwinder (model "UW1" by Graw GmbH & Co. KG, Nuremberg, Germany), which connects to the lifting balloon. The unwinder's primary function is to prevent the rope from entangling during release and ascent, ensuring a stable flight profile. The rope sets the distance between the balloon and the payload, which prevents interference from the balloon's turbulent wake. The helium-filled meteorological balloon TOTEX TA2000 is used to achieve the required lift. The typical payload mass is around 3.4 kg, although slight variations between flights can occur due to the use of ancillary materials like tape and insulation.

2.3.1 Power systems

The main system, including the Raspberry Pi and other core components, is powered by a battery rack consisting of four 5200 mAh lithium-ion cells. The Vaisala RS41SGP radiosonde is powered separately by two AA batteries. The ECC utilizes its own dedicated power source. Finally the POPS utilizes an additional 3500 mAh / 37.8Wh Li-ion battery pack. This main battery connects to the custom printed circuit board (PCB), which distributes stabilized voltages through power rails thanks to a voltage converter. The voltage converter needs to be adjusted to 12 V and 5 V to power the different instruments and sensors, ensuring each one receives the specific voltage it needs. The duration of a balloon sounding is typically shorter than the maximum operational time of the payload batteries, so battery life is not a constraint for this setup.

2.3.2 Control and processing

The central control and processing unit for the payload is a Raspberry Pi Model 3B+ single-board computer. To facilitate stable connections with the various instruments, the Raspberry Pi is augmented with a custom-designed PCB. This PCB interfaces directly with the Raspberry Pi's general-purpose input/output (GPIO) pins and provides the necessary 2,54 mm pin sockets and

https://doi.org/10.5194/egusphere-2025-5568
Preprint. Discussion started: 9 December 2025

Molex 6373 series for physical instrument integration. Accurate timekeeping, critical for data synchronization and preventing time drift, is maintained using a NEO-6M GPS module connected via USB. This module provides a Pulse-Per-Second (PPS) signal to the system, allowing for a high-accuracy system time.

2.4 Balloon operation

Flight operations, including instrument interfacing, data acquisition, storage, transmission, and synchronization are conducted during flight at the PCB. For data telemetry, the platform utilizes a Vaisala RS41SGP radiosonde. Initialization of the radiosonde before launch is performed using a Vaisala RI41 ground check device. Data packages are transmitted using the xData fields inside the Vaisala´s transmission protocol. While the radiosonde transmits packets at a constant frequency of 1 Hz, the data payload accommodates higher temporal resolutions by buffering multiple samples into a single transmission. For example, although the transmission rate is 1 Hz, UCASS data is encoded with two samples per packet, resulting in an effective 2 Hz resolution upon decoding. Independently of the transmission, a higher-resolution dataset is saved locally, with data from most instruments recorded at double their sampling rate. An exception is the UCASS, whose data is both transmitted and stored at 2 Hz. The transmitted data allows for live flight monitoring on the ground, while the stored data provides a comprehensive dataset for post-flight analysis. The monitoring was done in the Vaisala MW41 sounding system coupled with a CG31 antenna with a secondary antenna as a backup. This backup was done by the limitations of the main system, not build for simultaneous soundings allowing a continuous recording of any overlaping launches.

2.5 Data and sampling treatment

2.5.1 Data processing

The initial raw data is collected in 10-second bulk files, with all sensors in the same file. The first step requires consolidating the files into one file per flight. This processed raw data forms the Level 0.1 dataset, consisting of decentralized, files with invalid entries removed for each sensor operating under the SBC (e.g., impactors or UCASS). The Level 0.5 dataset is then generated by using RS41-SGP data to trim the Level 0 data, ensuring that each sensor's data spans the entire flight duration, from ascent to landing. Finally, the Level 1 dataset is created by performing data validation, including checksums, to produce a final file for each sensor that contains only valid data points for the entire flight.

2.5.2 Scanning electron microscopy

Particle characteristics were analyzed using a scanning electron microscope coupled with energy-dispersive X-ray spectroscopy (SEM-EDX). This technique allows for comprehensive analysis of individual particles, providing insights into their physical nature (size and shape) and chemical composition. Geometrical parameters were obtained directly from the SEM images, while chemical analyses are performed using the EDX system: For details on the procedure see Ebert et al. (2024)

For each individual particle identified via SEM imaging, an EDX spectrum was manually acquired to determine its elemental composition. The SEM-EDX technique is commonly used to analyze individual particles (Rades et al., 2014), especially

https://doi.org/10.5194/egusphere-2025-5568
Preprint. Discussion started: 9 December 2025

when the total sample mass is uncertain or subject to changing atmospheric conditions (Worobiec et al., 2010). The technique provides insights into the aerosol mixing state by analyzing individual particles (Bondy et al., 2018). It can differentiate between an external mixture, where particles of distinct composition coexist (e.g., an iron oxide particle next to a silicate particle), and an internal mixture, where multiple chemical species are present within a single particle (e.g., a soot core with a sulfate coating). This capability provides detailed information on sample heterogeneity, which is overlooked by bulk analysis techniques that average the composition of the entire sample. Understanding the mixing state is important, as it governs the aerosol's hygroscopic, optical, and chemical properties (Li et al., 2018), and thus its overall impact on climate and air quality (Gaston, 2020).

The elemental composition of each individual particle, focusing on major elements such as S, Na, Al, Si, K, Ca, Fe, or Pb, was determined from the EDX spectra. These compositions were then expressed as normalized atomic percentages. To ensure accurate quantification of the particle chemical composition, those elements originating from the substrate, specifically carbon (C), oxygen (O) and nitrogen (N), were excluded from the analysis. Apart from N being a compound of the substrate, N is also subject to a high degree of error in EDX detection, hence, this species (N) is also discarded from further analysis.

3 Application: field missions (BISTUM) in the years 2023 and 2024

The first part of the field campaign (BISTUM23) took place in August 2023 at Tailfingen, Albstadt, located in Baden-Württemberg, Germany (48.2576° N, 8.98619° E). Albstadt lies within the Swabian Jura, a low mountain range on the southern outskirts of the Alps, characterized by a high plateau with forested areas. This area is predominantly rural, well distanced from major industrial centers which results in a potentially low polluted atmospheric profile compared to densely populated basins (Manisalidis et al., 2020). The launch site was located at 886 m above sea level (ASL). The Albstadt area is a hotspot for thunderstorms because the regional landscape—specifically the interaction between wind flowing around the Black Forest and over the Swabian Jura—creates a natural trigger point for orographic convection (Kunz et al., 2022).

The second part of the field activities (BISTUM24) took place in June 2024 at Spielberg, Brachttal, located in Hessia, Germany (50.30519° N, 9.25899° E). Geographically, Brachttal is hilly area, with a dense tree mass coverage, northeast of the most densely populated part of the Frankfurt Rhine-Main region. This area is characterized, by a rural setting, although its position relative to the industrialized area of the Rhein-Main-region has potential for being affected by airborne pollutants. The launch site was located at 402 m ASL. Thanks to its moderate local background urban pollution convective transport of pollutants could be characterized (Moormann et al., 2025).

The flight overview for both field operations is included in the supplement (tables S5 and S6).

4 Results and Discussion

During the BISTUM23 campaign, a total of 16 flights were performed. The operational status of the key particle instruments UCASS and the impactors was evaluated, as detailed in the supplement. While many flights were successful, several en-

https://doi.org/10.5194/egusphere-2025-5568
Preprint. Discussion started: 9 December 2025

countered technical issues with individual components during flight. Some flight datasets were unable to be recovered due to corrupted telemetry and physically irretrievable payload.

Learning from the initial deployment, adjustments were made before the second campaign, which consisted of 12 flights. The complete success rate was about 60% for BISTUM24 campaign. A summary of the instrument failures during this initial campaign is presented in the electronic supplement. For the present study, the flight from 14th of June 2024 was specifically selected as it represents a baseline case under non-convective conditions, as an example for the capabilities of the payload. This choice allows for a clear characterization of aerosol nucleation processes without the complexity of deep convection. Furthermore, this flight exhibited the highest data quality of all available datasets, with few invalid data packages as well as samples from the impactors. This analysis therefore serves as a reference for our ongoing investigation into the more complex convective cases.

4.1 Synoptics and flight conditions

The synoptic situation on the 14th of June 2024 was influenced by a low pressure system located north of Great Britain (Fig. 2). Germany was under influence of a trough with a weak pressure gradient. The warm front was approaching Frankfurt from the east inducing vertical transport and winds northeastward of Frankfurt towards Brachttal, driving pollutants to the middle sections of the troposphere. The profile indicates a stably stratified atmosphere, with convective available potential energy CAPE near to 0 Jkg^{-1} (0.15 Jkg^{-1}) (Stull, 1988).

The balloon-launch took place at 1400 UTC. During payload preparations, temperatures at ground level were 14°C with relative humidity of 74% and windspeed of around 1.5 ms^{-1} from SW. The balloon-probe's ascent finished at 30860 m ASL at 1505 UTC when the balloon burst. Around 1645 UTC LOONIS landed and was recovered immediately. After a check whether the impactor pumps had worked during sounding, impactor samples were stored to avoid unintentional contamination. The profile acquired (Fig. 3) shows a water saturated region between 900 and 800 hPa.

4.2 Instrument Performance and Data Validation

The UCASS utilizes an open-path design without moving parts, relying on the balloon's ascent rate to draw air through the sampling volume. This method has been enhanced by incorporating a thermal flow sensor (TFS) to obtain a local measurement of the instrument's internal sample flow speed, which was calibrated with a pitot tube (Jost et al., 2025). The TFS provides a direct and responsive measurement of the internal flow velocity, capturing instantaneous fluctuations that are not resolved by GPS-derived platform velocity. Relying on the instrument platform's velocity introduces uncertainty, especially during rapid ascents (up to 6 ms^{-1}), and is a source of error when considering particle inertia. The resulting signal is highly responsive and can capture instantaneous fluctuations in the internal flow (Jost et al., 2025). The two independent TFS units are strongly correlated with each other, both exhibit significant scatter and deviation when compared against the GPS-derived speed (Fig. 4). This suggests the TFS provides a more self-consistent measurement of local flow. In contrast, the limited frequency and high variability of GPS-derived flow, especially during rapid ascents (up to 6 ms^{-1}), create uncertainties in particle counts. The TFS method shows large scattered deviations relative to the GPS-derived flow exceeding $\pm$30% (Fig. 5).

https://doi.org/10.5194/egusphere-2025-5568
Preprint. Discussion started: 9 December 2025

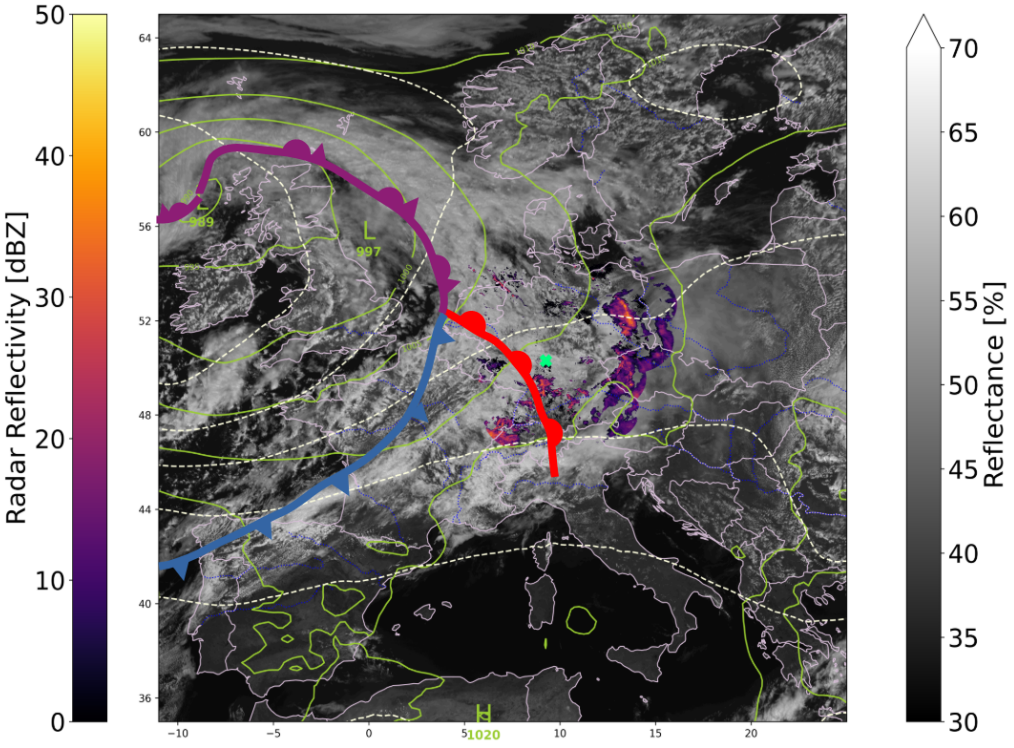

Figure 2. Surface pressure (green-yellow lines) and 500 hPa geopotential (dashed lines) from ERA5 (Hersbach et al., 2020) in central Europe on the 14th of June 2024. The background shows high-resolution visible (HRV) channel imagery from MSG Seviri, with RADOLAN radar reflectivity overlaid for Germany. Relevant fronts, based on the pressure field and DWD analysis (Deutscher Wetterdienst, 2024), are also depicted. The next day, a warm and a cold front crossed over the measurement location (green cross), changing from clear skies to increased cloud coverage with precipitation.

The UCASS intercomparison reveals a significant discrepancy between the two units (Fig. 6). One instrument consistently reports higher particle number concentrations, a scatter that becomes most pronounced in high-concentration environments. This suggests a systematic, instrument-specific overestimation. However both units responded simultaneously to the environmental changes, confirming the presence of the saturated air layer observed by the humidity sensor.

This uncertainty must be taken into account when considering inertia as a source of miscounts, particularly for particles with $D_p > 1$ μm. This effect becomes significant under two conditions: first, during any change in the instrument's velocity or direction, and second, when a non-zero Angle of Attack (AOA) occurs. A non-zero AOA indicates that the airflow is not parallel to the instrument's axis, making the flow non-isokinetic. While non-isokinetic flow may be negligible for particles smaller than 1 μm (Arouca et al., 2010), it leads to less reliable counting for larger particles (Brem and Zhang, 2008). Larger particles have significant inertia. Under non-isoaxial sampling conditions, this inertia, combined with complex internal airflow, can cause them to impact and deposit onto the UCASS's inner walls instead of reaching the measurement volume (Jost et al.,

https://doi.org/10.5194/egusphere-2025-5568
Preprint. Discussion started: 9 December 2025

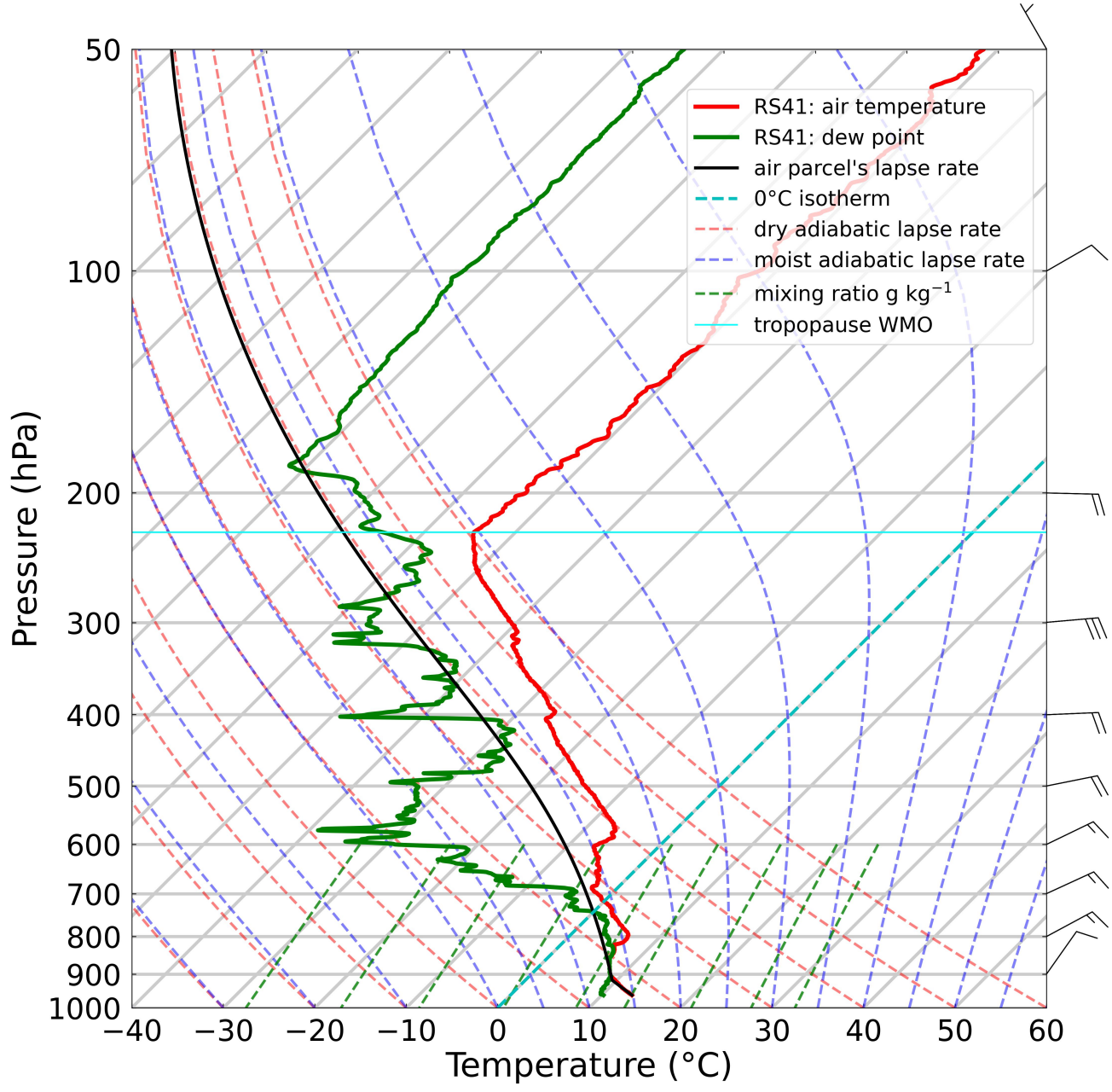

Figure 3. SkewT diagram depicting the vertical profile of atmosphere's thermodynamic conditions during BISTUM24 campaign on 14th June 2024. The launch time was at 14:00 UTC. The observed near-zero CAPE index (1.6 J per kg) confirms the absence of significant convective instability.

https://doi.org/10.5194/egusphere-2025-5568
Preprint. Discussion started: 9 December 2025

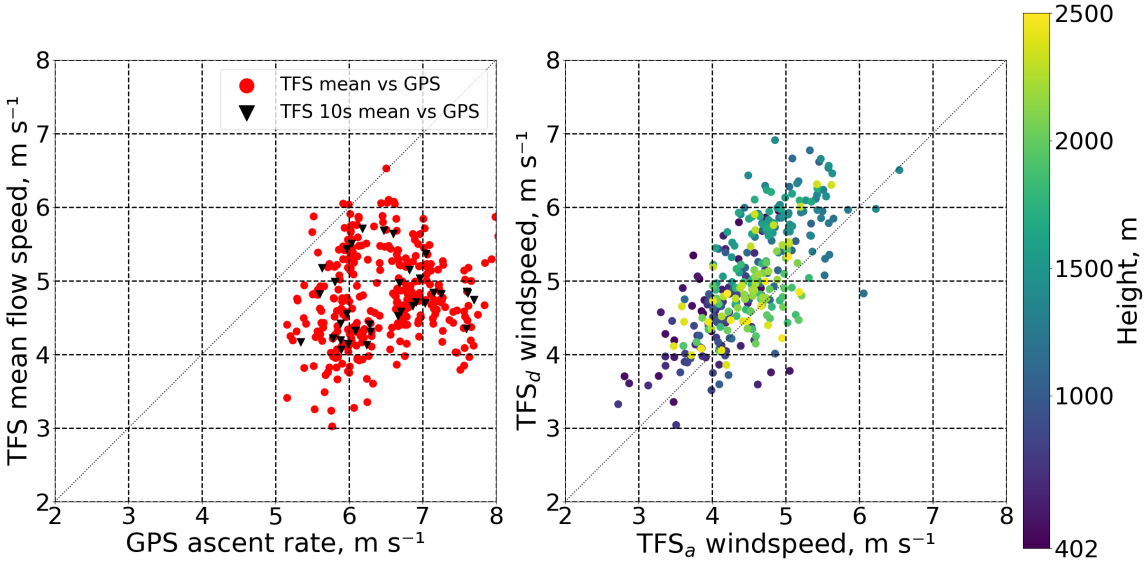

Figure 4. Comparison of wind speed measurements from three different sources observed on 14 June. The leftplot compares TFS1 and TFS2 against GPS, the right plot compares the two TFS. The altitude of the compared measurement is color coded.

2025). This deposition is more probable for particles with $D_p > 1$ μm because their mass is sufficient to cause deviation from the streamlined airflow within the curved nozzle. This deposition leads to under counting. By using TFS data to calculate the sampled volume, these errors are minimized because the calculation relies on a velocity value that is closer to the true, instantaneous velocity of the air passing through the UCASS.

The LWC derived from the UCASS during the cloud pass reached a peak values of 3.23 and 2.44 g m^{-3} (Fig. 7). This is an order of magnitude higher than from the typical range of 0.1-0.2 g m^{-3} (Misumi et al., 2018) reported for continental stratocumulus clouds in previous in-situ and modeling studies (Baumgardner et al., 2011; Noh et al., 2013). Although these values are not directly comparable, as the cited works serve as a reference for typical LWC in similar continental stratocumulus clouds rather than a simultaneous measurement. Using Moderate-resolution Imaging Spectroradiometer (MODIS) cloud liquid water path data from the 14th of June the LWC values for the cloud layer (1 Km) would fall between 0.1 and 1.1 g m^{-3}. The direct comparison from the LWC as well as the particle concentration points towards overestimated measurements. This overestimation does not appear to be an artifact of sizing range truncation. The instrument measuring range, with upper limits of 32.5 μm and 51.5 μm, is nominally sufficient to detect the full population of typical cloud droplets, which can grow to 50 μm (Pruppacher and Klett, 2010). The cloud effective radius from MODIS data shows a median droplet size of about 25 μm which overlaps with the mean peak of the size distribution observed in the UCASS data.

The volume of an individual water particle increases with the cube of its diameter (D^3). While smaller particles are typically far more numerous, this scaling means that the relatively few larger particles in the size distribution often contain a disproportionate amount of water. As a result, these larger particles frequently make the dominant contribution to the total LWC. This

https://doi.org/10.5194/egusphere-2025-5568
Preprint. Discussion started: 9 December 2025

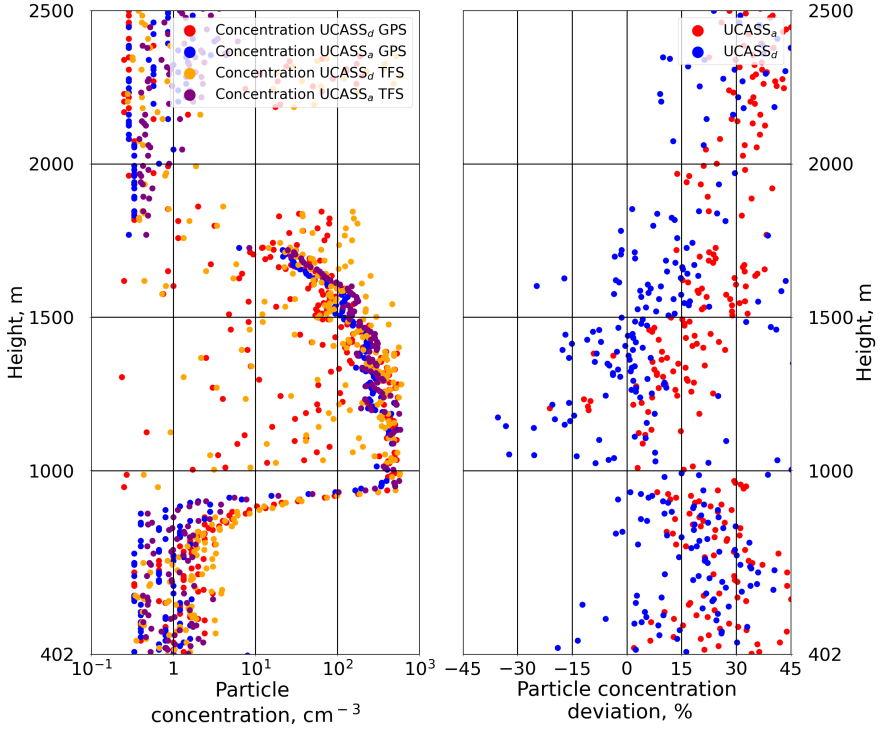

Figure 5. Comparison of two methods for calculating particle number concentration from a balloon flight on 14th of June. The left panel shows the absolute concentration profiles derived using a GPS-based ascent rate versus a TFS measurements (orange, purple dots). The right panel shows the percentage deviation of the TFS method relative to the GPS method of each unit (UCASSa and UCASSd).

aligns with the report of Schön et al. (2024), who noted that the UCASS recorded higher number concentrations than other OPCs in the 2.12–2.36 μm diameter range. Despite particle truncation, the net LWC is overestimated, implying an error that inflates particle volume. A plausible explanation is the overcounting of particles, as artifacts from droplet shattering are known to be a significant issue for airborne probes in cloudy conditions (Spanu et al., 2020; Huang, 2021). Although limitations in our instrumentation preclude a fully quantitative analysis, our results show a clear trend of increased cloud droplet number concentration under higher particle loading. This observation is qualitatively consistent with the Twomey effect, a foundational principle of aerosol-droplet interactions in boundary layer clouds (Yang et al., 2019).

Therefore, while the UCASS is suitable for identifying the vertical structure of aerosol layers, its quantitative accuracy is reduced in high-concentration environments. Despite these quantitative uncertainties, Schön et al. (2024) found similar vertical particle size distribution patterns between the UCASS and other OPCs, indicating that the overall structure of aerosol layering can still be reliably captured. This capability is critical for process studies, such as investigating the impact of aerosols on cloud condensation nuclei (CCN) populations and subsequent cloud properties (Heutte et al., 2025).

https://doi.org/10.5194/egusphere-2025-5568
Preprint. Discussion started: 9 December 2025

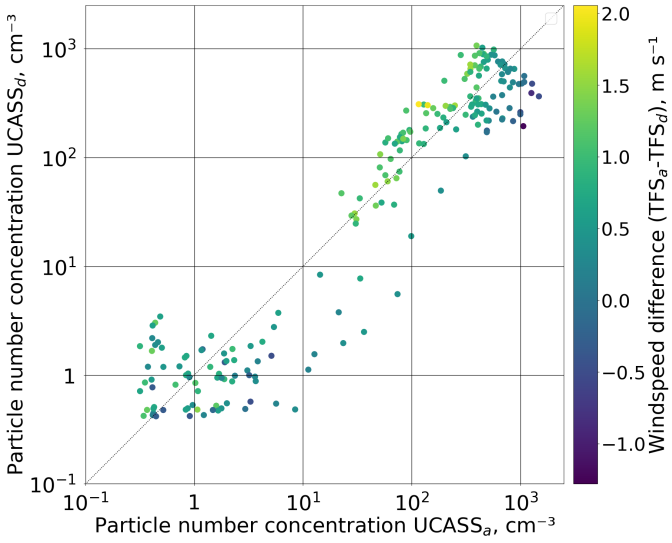

Figure 6. Particle number concentrations from two UCASS instruments measured on 14 June within a saturated air layer. Data points are colored by GPS altitude, with concentrations calculated using True Flow Speed (TFS).

4.3 Vertical Aerosol Distribution and Cloud Microphysics

The total particle number concentration was derived by summing the counts per second across all size bins and dividing by the volumetric flow rate. The vertical profile (Fig. 8), at a 1 Hz resolution corresponding to approximately a 6-meter vertical resolution, reveals that the concentration profiles from both instruments demonstrated strong qualitative agreement, capturing similar trends throughout the ascent.

During the initial 600 m of ascent, significant particle concentrations were detected in both water-saturated and unsaturated air parcels. This period of high particle loading was visually corroborated by video footage showing a noticeable decrease in visibility, indicative of water condensation on aerosols. Within the saturated air parcel, between 1000 m and 2000 m ASL, particle concentrations reached values up to 1000 particles per cm^3 before subsequently decreasing with increasing altitude to approximately 50 particles per cm^3.

The vertical size distribution profile (Fig. 9) shows a noticeable structure between 1500 m and 2000 m for both instruments. The combination of the observed altitude, water saturation, and particle concentration indicates the presence of a boundary layer cloud. The size distribution shows two different behaviors based on humidity. Saturated air parcels exhibit a particle concentration between 700 and 900 particles per cm^3, featuring a size distribution that peaks at roughly 20 μm (UCASSa/b). The agreement between the two UCASS units supports the reliability in saturated conditions; conversely, in air parcels not saturated with water vapor, the low particle concentrations (approximately 1 particle per cm^3) lead to higher statistical uncertainty across the entire size distribution.

https://doi.org/10.5194/egusphere-2025-5568
Preprint. Discussion started: 9 December 2025

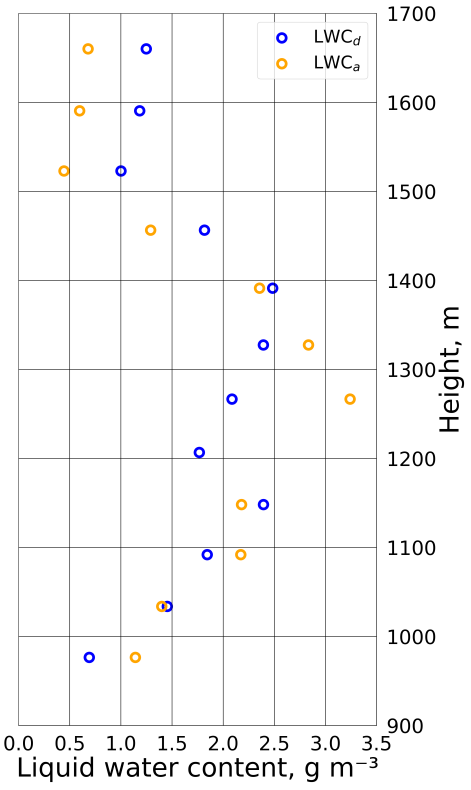

Figure 7. Comparison of UCASS derived LWC on June 14th. UCASS LWC is calculated from droplet measurements assuming spherical shape and water density of 1 g per cm^3.

The distinct particle size detection ranges of the POPS and UCASS units allow for a direct comparison between activated and inactivated particles. During the boundary layer pass, the size distribution exhibits a bimodal pattern (Fig. 10). For particles with diameters ranging from 0.3 μm to 2.6 μm, the size distribution behavior is consistent with previous observations (Liu et al., 2021) until the saturated region is reached.

This saturation triggers a distinct divergence between the two instrument types. Upon entering the water-saturated region, the aerosol concentration observed by the POPS decreased abruptly by 90% over a vertical transition of 100 m (visible in Fig. 8). Simultaneously, the UCASS units recorded a concentration peak, increasing from 10 to 800 particles per cm^3. This pattern is a direct in-situ observation of aerosol-water activation. Hygroscopic aerosol particles measured by POPS (0.14–2.4 μm) take up water and grow sufficiently to become cloud droplets (Abdul-Razzak and Ghan, 2000; Pöhlker et al., 2023). As they grow beyond the upper detection limit of the POPS, they are recorded by the UCASS.

While the UCASS may overestimate absolute number concentrations (as discussed in section 4.2), the qualitative bimodal trends are consistent with established microphysical principles (Pruppacher et al., 1998). Specifically, the presence of a bimodal cloud particle distribution has been shown to arise from the different activation properties of distinct, externally mixed aerosol

https://doi.org/10.5194/egusphere-2025-5568
Preprint. Discussion started: 9 December 2025

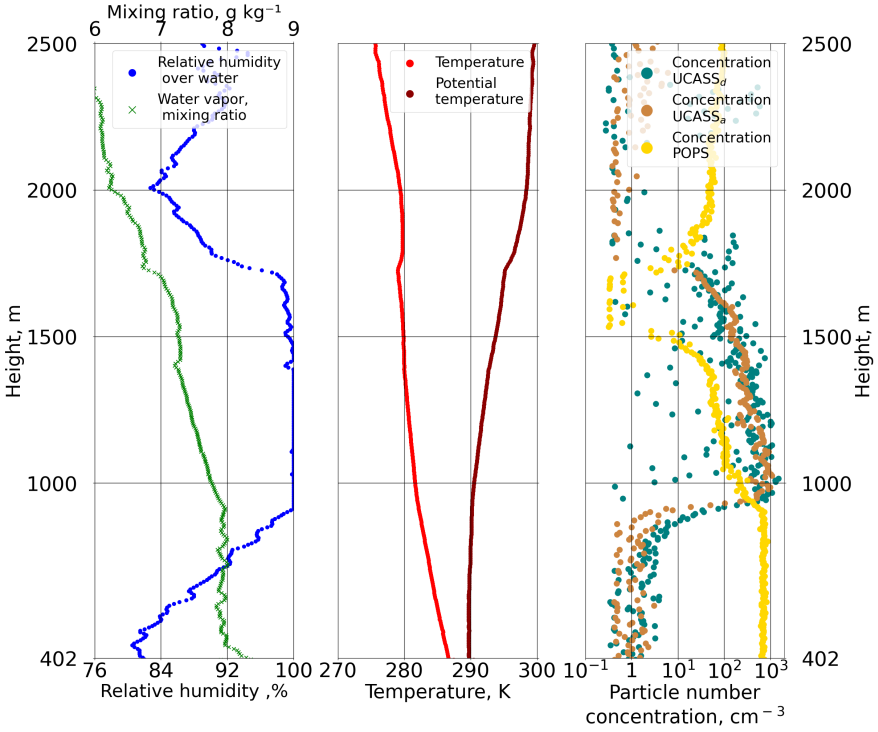

Figure 8. The data shows a well-defined planetary boundary layer capped by a strong temperature inversion with its base at approximately 850 m, as seen in the potential temperature profile. This inversion traps moisture, leading to saturation (RH $\approx$ 100%). Consequently, aerosol particles activate into cloud droplets, causing the measured particle concentration to increase by over an order of magnitude. Potential temperature is calculated based on (Baumgartner et al., 2020).

populations (Jacobson, 2003). Jacobson showed through modeling that aerosol types with different chemical compositions and solubility activate at different diameters. The smaller sizes observed by POPS (0.14–2.4 μm) are comparable to Jacobson's modeled 0.1–0.5 μm mode, while the larger UCASS mode corresponds to the activated droplet mode (5–10 μm in theory, observed here near 20 μm). This activation-driven growth is transient; as the relative humidity drops below 95%, the UCASS peak disappears and the POPS concentrations recover, signifying the evaporation of these newly formed droplets.

The complementary nature of the POPS and UCASS measurements, with their distinct particle size detection ranges, allows for a comprehensive assessment of this phenomenon, aligning with fundamental principles of cloud microphysics, where the availability and properties of cloud condensation nuclei (CCN) govern the initial stages of cloud formation (Seinfeld and Pandis, 2016).

4.4 Aerosol Chemical Composition and Source Attribution

The impactor system operated as planned throughout the flight, collecting particulate samples according to the pre-programmed sampling schedule. During flight, the INA219 power monitor recorded the voltage and current supplied to the pumps. The

https://doi.org/10.5194/egusphere-2025-5568
Preprint. Discussion started: 9 December 2025

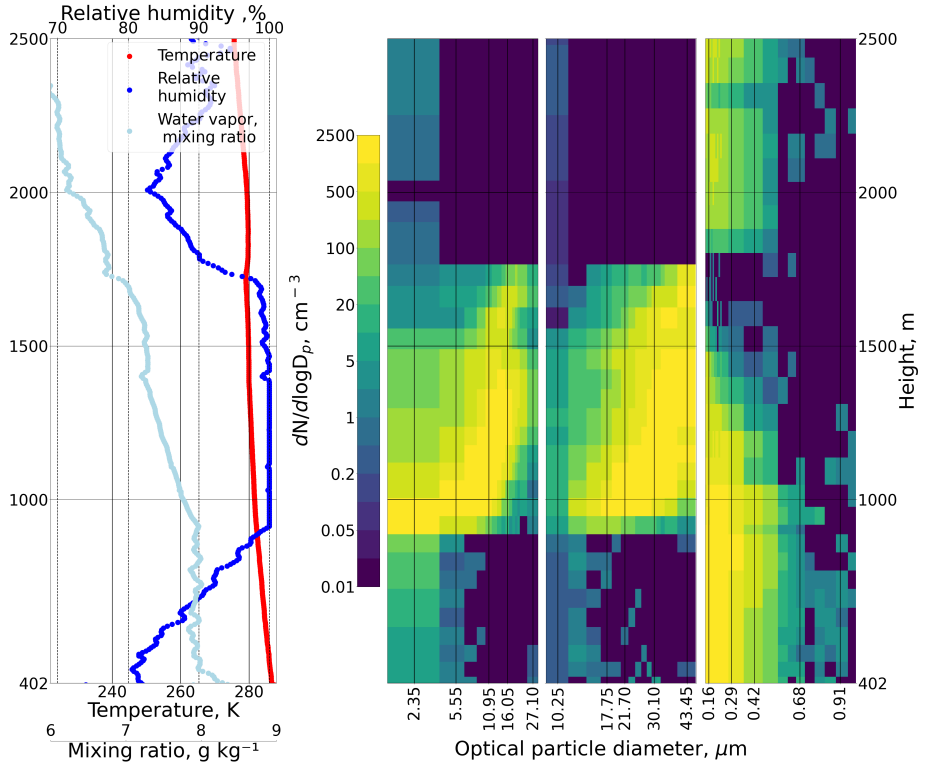

Figure 9. Vertical profiles of temperature, relative humidity and water vapour mixing ratio (left) and particle size distribution observed on 14 June 2024. UCASSa, UCASSd (middle) have an optical particle diameter of 1.51 μm and POPS (right) of 1.41 μm.

resulting power consumption remained within the nominal operational range, indicating that the pumps were functioning as intended (see 2.2.3). This was also confirmed by the power consumption of the system, matching the power drainage observed during the laboratory testing.

The first impactor collected particles across a vertical profile extending from 500 m to 4500 m. This transect passed through a saturated atmospheric region, with in-cloud conditions identified between approximately 1000 m and 2000 m ASL. Consequently, the collected sample represents an integration of aerosols from different atmospheric layers, below the cloud, the cloud layer itself, and the free troposphere above, until end of sampling. Within the cloud layer, the sample is expected to contain a mixture of interstitial aerosols and cloud residuals—the non-volatile nuclei remaining after droplet impaction and evaporation. While this integrated sample does not isolate particles that acted as CCN, its analysis provides insights into the properties of the aerosol population that was available for cloud droplet activation.

The samples revealed a heterogeneous mixture of particles with diverse morphologies, sizes, and chemical compositions. A well-mixed atmospheric layer is characterized by a relatively uniform (homogeneous) aerosol population due to turbulent mixing over time. Therefore, the observed heterogeneity indicates that the sampled layer was not well-mixed. This variety of particle types strongly suggests a recent convergence of different air masses, each carrying a distinct aerosol signature from

https://doi.org/10.5194/egusphere-2025-5568
Preprint. Discussion started: 9 December 2025

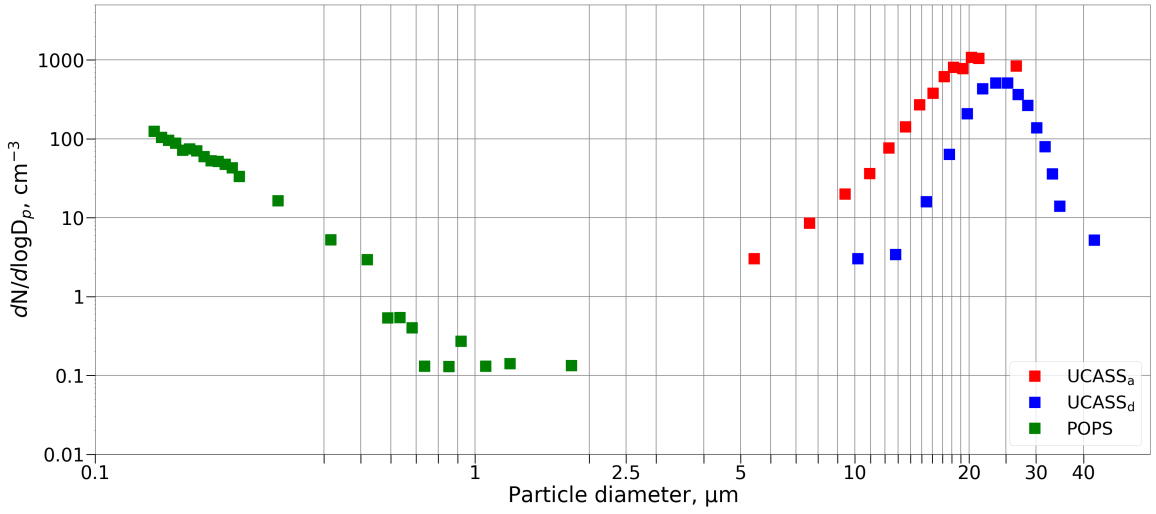

Figure 10. Particle size distribution, normalized by the logarithmic bin width, measured by Optical Particle Counters (OPCs) over Spielberg, Germany, on 14th June 2024, during the BISTUM24 campaign. The distribution represents a one-minute average during a cloud transect between 1761 m and 1817 m altitude. Ambient conditions were 280.2 K and 100% relative humidity.

its region of origin. The presence of such a varied mixture points toward a complex atmospheric structure where air parcels influenced by sources like urban pollution coexist with other air masses that have not had sufficient time to homogenize.

The sampled particles show significant diversity in their chemical composition and morphology, as shown in Fig. 11 and Fig. 12. The aerosol population contained a complex mixture including iron-rich (Fe) agglomerates (Fig. 11a), calcium rich particles (Fig. 11b) and alumino-silicate mineral dust (Fig. 11c). The sampled air layers contained ammonium sulfate (Fig. 12) a defining characteristic of aged continental aerosol populations (Pöschl, 2005; Morgan et al., 2010).

To trace back the origin of the particles Lagrangian back trajectory calculations have been conducted, displayed in (Fig. 14). The backward trajectories were initiated every minute during the flight at the respective positions in space and time. Meteorological information, especially the wind velocities were obtained from the ICON-D2 weather model analysis data with a horizontal spatial resolution of approx. 2 km and vertical resolution of between 30 - 100 m in the lower troposphere. The temporal resolution of the data is 3 hours, for time steps in between a linear interpolation has been selected. The Lagrangian tool is a tailored algorithm, performing linear interpolation in space to determine the respective wind velocities transporting the air parcels. The trajectories are calculated backwards in time for 24 hours or until the parcels left the domain of the ICON-D2 operational model. In case of a particular event (like a Saharan dust event intrusion) not only is it possible to get the spectral signature but the path that the sampled air mass followed, enhancing the information that the particles provided. The back trajectories indicate that the sampled air masses traversed the anthropogenically influenced Rhein-Main metropolitan area. The chemical composition of these particles, identified by EDX, as primarily ammonium sulfate $(NH_4)_2SO_4$, is a direct consequence of the atmospheric processing of pollutants from the upwind source region. The back trajectories (Fig. 14)) confirm that the sampled air masses traversed the anthropogenically influenced Rhein-Main metropolitan area. Consequently, emissions

https://doi.org/10.5194/egusphere-2025-5568
Preprint. Discussion started: 9 December 2025

from industrial processes, dense traffic, and agricultural lands in this region likely serve as the primary sources for the observed particles (Birmili et al., 2016). First, sulfur dioxide (SO_2), emitted from industrial activities and fossil fuel combustion in the Rhein-Main area, is oxidized in the atmosphere to form sulfuric acid (H_2SO_4). Emissions from industrial processes, dense traffic, and surrounding agricultural lands in the Rhine-Main region serve as the primary sources for these particles (Birmili et al., 2016). This aligns with airborne measurements across North-Western Europe, which show that the sub-micron aerosol burden in polluted air masses is dominated by secondary components like ammonium nitrate, organic matter, and sulfate (Morgan et al., 2010).

It is important to note a potential sampling artifact identified with the current impactor setup. During the SEM analysis, a population of non-volatile, P-K-rich particles (Fig. 13), which also contained minor amounts of K, Na, and Mg, was identified. These particles are considered artifacts. This classification is based on their distribution across the sampling substrate; unlike other particle types, they were not concentrated in the impaction spot but were also found on the substrate edges. Furthermore, they appeared on more than half of the flown samples but were absent from laboratory blanks. The source of this contamination remains under investigation, but it is hypothesized that these particles may enter the impactor via diffusional processes during the payload's turbulent descent, bypassing the intended collection stage. However, because these P-K-rich particles can be unambiguously identified by their unique composition and distribution, they do not bias the overall analysis of the targeted aerosol populations.

While SEM analysis is useful for characterizing the physicochemical properties of individual particles, this manual method is limited to a small number of particles. Consequently, it lacks the statistical power required to definitively establish the relative abundance of different particle types acting as CCN within a cloud event. Determining the dominant aerosol population serving as CCN depends on analyzing a much larger number of collected cloud residual particles to enable a statistically robust characterization (Kandler et al., 2007a, 2018). For this particular case study, the number of analyzed particles is insufficient to extract all relevant chemical properties of the cloud CCN, but a measurement strategy involving more frequent sampling on short notice could provide the necessary statistics in future investigations.

4.5 Evaluation of Trace Gas Sensors

To characterize the payload's operational performance distinct from the aerosol analysis, we examine the trace gas profiles in the lower troposphere (Fig. 15). Both the CO (smoothed with a 30-second running average) and O_3 signals exhibit a coincident local maximum at approximately 1000 m, identifying the cloud base. While this detection confirms the sensors' ability to locate strong atmospheric gradients, the subsequent measurements reveal significant instrumental artifacts. The following discussion details the specific limitations of the electrochemical CO sensor under these rapid ascent conditions.

The operational characteristics of the CO sensor introduce significant uncertainties when deployed on rapidly moving platforms. The sampling strategy is a critical factor when comparing datasets from different measurement platforms (Kezoudi et al., 2021). Stationary (ground-based) and slow-moving platforms can sample a specific air mass under relatively stable or slowly evolving conditions (Chan et al., 2021; Moormann et al., 2025). In contrast, fast-moving airborne platforms, such as research aircraft or ascending weather balloons, encounter rapidly shifting temperatures, pressures, and humidity levels.

https://doi.org/10.5194/egusphere-2025-5568
Preprint. Discussion started: 9 December 2025

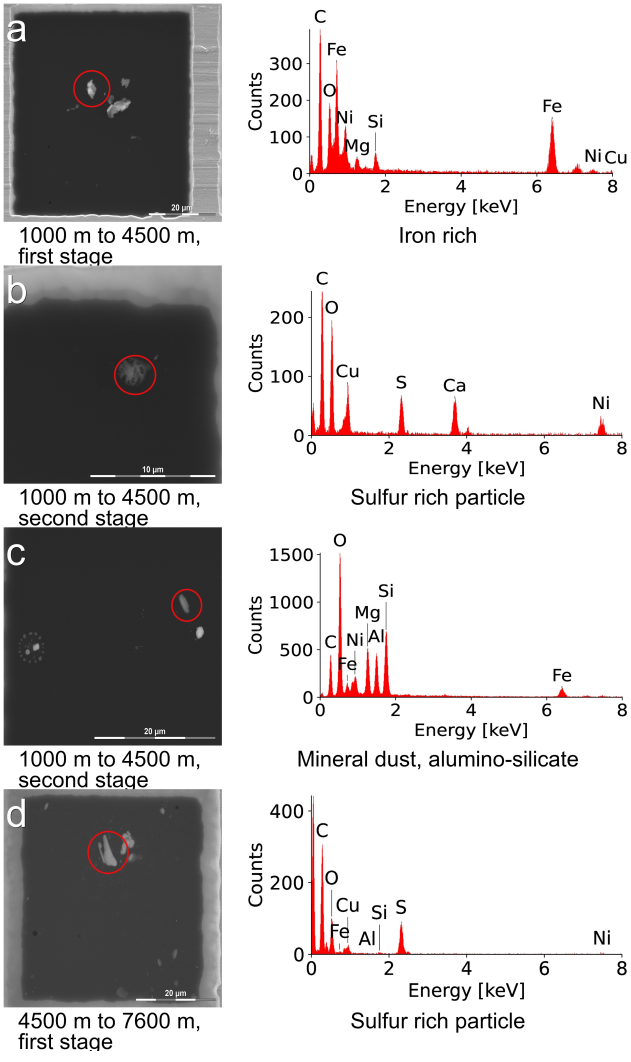

Figure 11. Examples of individual aerosol particles collected by the dual-stage impactors during the BISTUM24 flight on 14th June 2024, analyzed via SEM and EDX. The panels display the chemical heterogeneity of the sampled aerosol particles. Particles collected as cloud residuals by the first impactor (500-4500 m) include (a) an iron-rich agglomerate likely from industrial or traffic sources, (b) an aged secondary sulfate particle, and (c) an alumino-silicate mineral dust grain. Particles from the free troposphere (4500-7600 m) are shown in (d) illustrating complex, internally mixed aerosols characteristic of aged continental air masses.

https://doi.org/10.5194/egusphere-2025-5568
Preprint. Discussion started: 9 December 2025

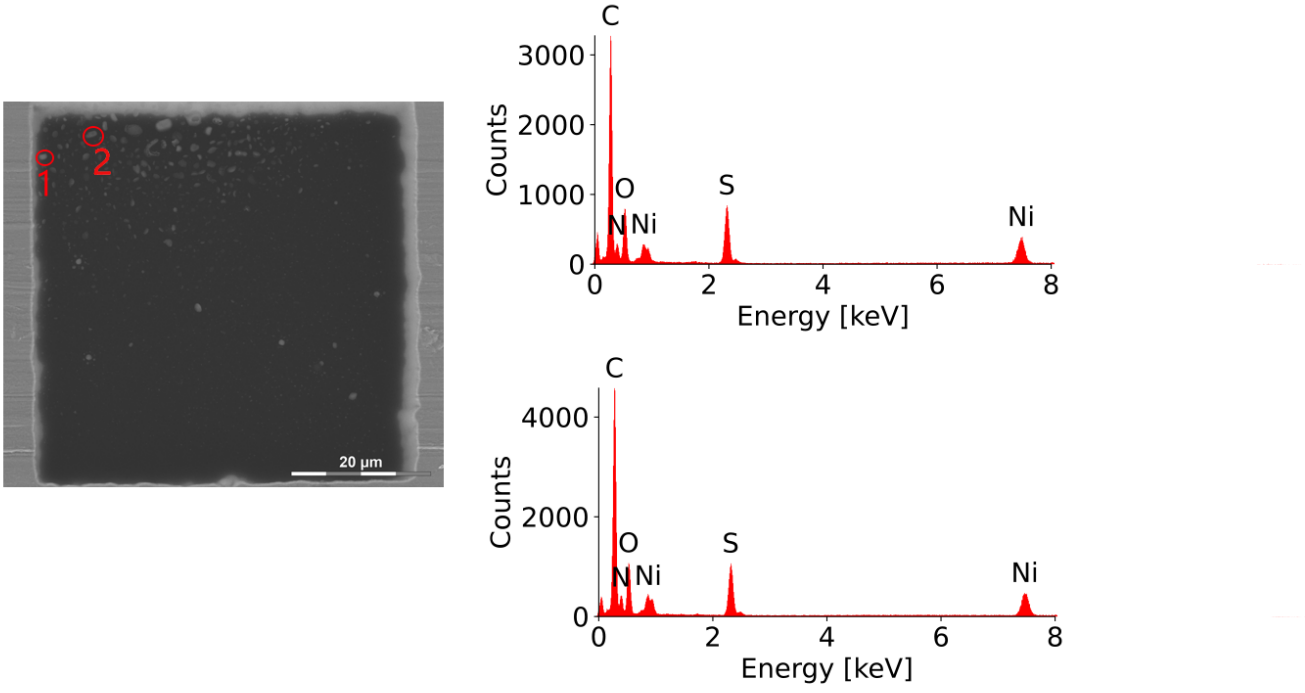

Figure 12. Example of an impaction spot collected by the dual-stage impactors during the BISTUM24 flight on 14 June 2024. The panels display particles on a collection grid, with selected particles highlighted for EDX analysis. The corresponding EDX spectra for points 1 and 2 reveal elemental signatures of Nitrogen (N), Sulfur (S), and Oxygen (O), consistent with a composition of nearly pure ammonium sulfate ($NH_4)2SO_4$. The presence of ammonium sulfate, a secondary aerosol species, indicates that the sampled air mass has undergone significant atmospheric aging.

This particular challenge is central to the performance of the electrochemical CO sensor used in this study. Manufacturer specifications indicate that such sensors require sufficient time to equilibrate and are designed for optimal performance under relatively constant pressure (Alphasense, 2019). The Alphasense CO-B4 sensor has a response time (t_90) of less than 30 seconds for a 10 ppm step change. Given the platform ascent rate (6 ms^{-1}) it traverses a vertical distance of approximately 180 m during the sensor's response interval. Consequently, the measurements will exhibit a significant vertical lag and represent a smoothed, rather than discrete, vertical profile. This limits the vertical resolution of the gathered data. These limitations are particularly pronounced in humid conditions. These limitations are particularly pronounced in humid conditions, with Relative Humidity >85%, the sensor output became erratic and non-physical. We observed raw signal saturation (reaching the sensor's voltage limit) and calculated concentrations ranging from -188 ppb to +803 ppb, with frequent excursions into negative values (down to -800 ppb in drier segments). This breakdown in linear response confirms that the sensor's electrochemistry is compromised by rapid moisture changes, rendering the data in these layers unusable for scientific analysis. The successful use

https://doi.org/10.5194/egusphere-2025-5568
Preprint. Discussion started: 9 December 2025

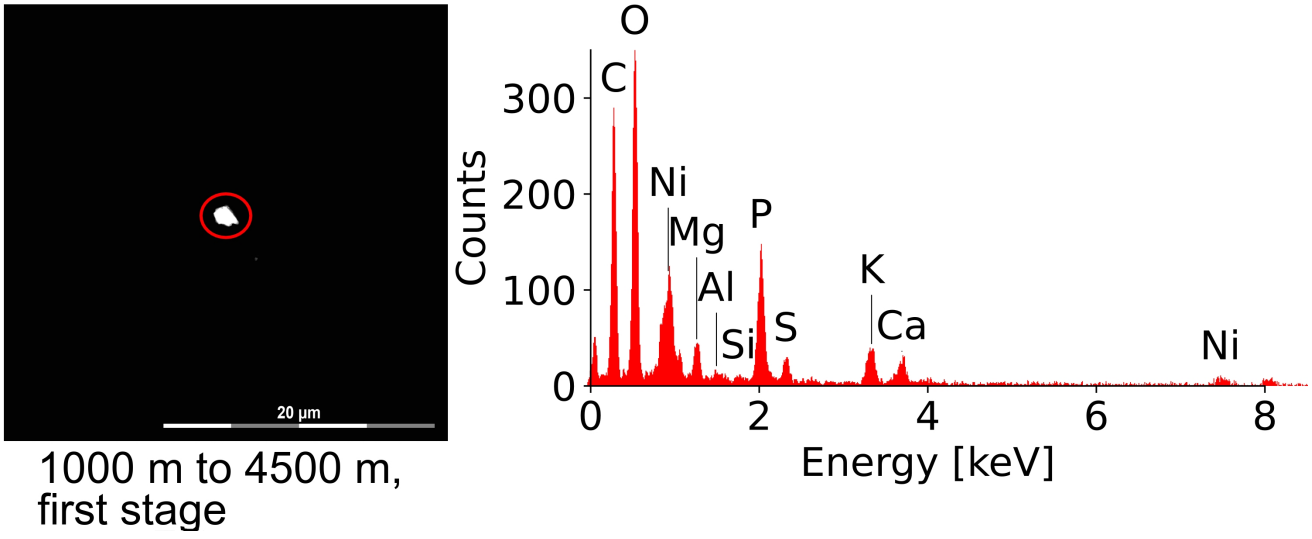

Figure 13. Example of an impaction spot collected by the dual-stage impactors during the BISTUM24 flight on 14 June 2024. The panel displays an example of a collected particle for EDX analysis. The corresponding EDX spectra for points 1 and 2 reveal elemental signatures of Potasaium (K) and Calcium (Ca).

of similar sensors on tethered balloon platforms, which permit slow profiling and stationary measurements at various altitudes, highlights the critical role of platform stability in obtaining reliable data (Han et al., 2021).

Conversely, the ozone profile displayed in (Fig. 16) shows the characteristic stratospheric ozone layer peak, with a sharp decrease towards the surface and a potential secondary peak in the lower stratosphere, reflecting photochemical production and destruction mechanisms. To assess its variability, the ozone profile from June 14th was compared at fixed pressure levels against the campaign-average ozone profile, revealing significant deviations from the mean. The deviation indicates a dynamically active and vertically stratified atmosphere. In the stratosphere, between 20 km and 30 km, a consistent positive anomaly in ozone partial pressure, with values up to +1 mPa, is observed. This suggests an enhancement of the stratospheric ozone concentration relative to the seasonal mean (Fig. 16).

The plot shows that the troposphere was not well-mixed. Instead, it was composed of distinct layers, including a notable band between 3,000 m and 7,000 m with significantly less ozone than the monthly average. A prominent ozone-rich layer, with a positive partial pressure anomaly reaching +4 mPa, is present at an altitude of 11-12 km. This feature could be a product of stratospheric intrusion, where filaments of ozone-rich air and drier air (RH is <10% between 11-12 km) are transported from the lower stratosphere into the troposphere, a process frequently observed over Central Europe (Trickl et al., 2018; Stohl et al., 2003). Such events are driven by specific large-scale meteorological patterns (Sprenger et al., 2003). In contrast to this ozone-rich layer, an ozone-poor air mass is observed at 5 km, identified by a strong negative anomaly of -1.2 mPa. The presence of

https://doi.org/10.5194/egusphere-2025-5568
Preprint. Discussion started: 9 December 2025

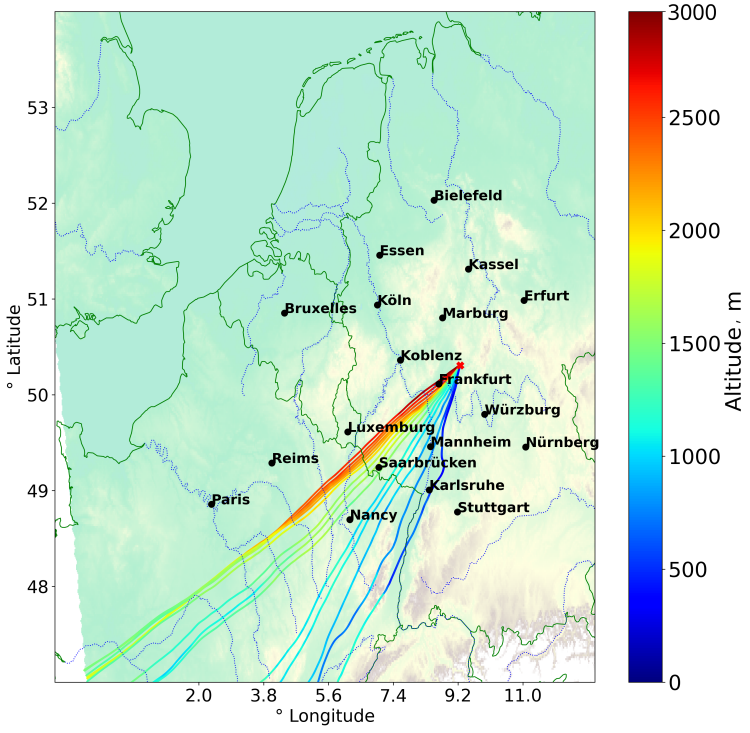

Figure 14. 24-hour backward trajectories for air masses sampled by the first impactor on 14 June 2024. The trajectories were initiated at various altitudes corresponding to the first two thousand meters of the LOONIS balloon sounding. The trajectory shows how air masses pass over the densely populated Rhine-Main metropolitan area. This air mass history suggests a strong potential for influence from anthropogenic emissions on the measurements.

these distinct layers, representing significant deviations from the typical seasonal variability (Thouret et al., 2006), indicates that the vertical ozone structure on this day was influenced by dynamic transport processes.

5 Conclusions

The BISTUM campaigns have demonstrated the proof of concept of the LOONIS platform. The strength of the payload lies in its modular adaptability to the shifting conditions of intense operation periods. This capability was demonstrated in the case study of the high-resolution observation of an aerosol activation event, evidenced by the data from the POPS and UCASS instruments. While POPS measured the depletion of accumulation mode particles, the UCASS simultaneously captured the resulting population of newly formed cloud droplets, which were outside the upper detection limit of the POPS. Crucially,

https://doi.org/10.5194/egusphere-2025-5568
Preprint. Discussion started: 9 December 2025

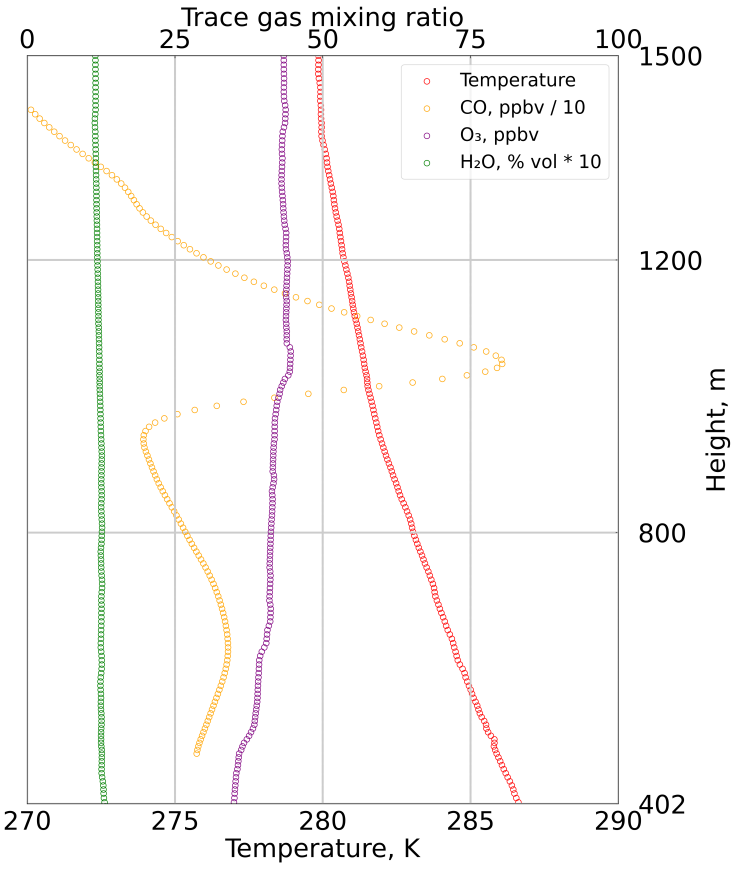

Figure 15. Vertical profiles showing trace gas trends and temperature within the lowest kilometer, observed on 14 June 2024. To fit on the same scale, the CO mixing ratio in ppbv has been divided by 10, and the H_2O in volume % has been multiplied by 10.

480 the platform's integrated approach does not end with in-situ data. Subsequent SEM-EDX analysis of particles collected by the impactors revealed a chemically diverse aerosol population, including aged industrial pollutants and mineral dust. Combined with back-trajectory analysis, these findings linked the aerosol sources to the heavily industrialized Frankfurt metropolitan area, providing a characterization from source to cloud process.

This synergistic dataset provides insight into process-level view of aerosol-cloud interactions. While the UCASS may over-
485 estimate absolute concentrations, its qualitative trends are reliable, and the methodological improvement of integrating a TFS enhances the accuracy of the particle concentration data compared to methods relying on ascent rate alone. The balloon's slow ascent is advantageous, providing the high vertical resolution needed to capture the evolution of aerosol activation over its vertical scale. This level of process detail within a single developing cloud profile would be difficult to resolve with faster-moving platforms like research aircraft.

490 However, these campaigns also served to identify critical limitations and guide improvements for future deployments. While the UCASS captured the formation of cloud droplets, it may overestimate absolute number concentrations. This phenomenon

https://doi.org/10.5194/egusphere-2025-5568
Preprint. Discussion started: 9 December 2025

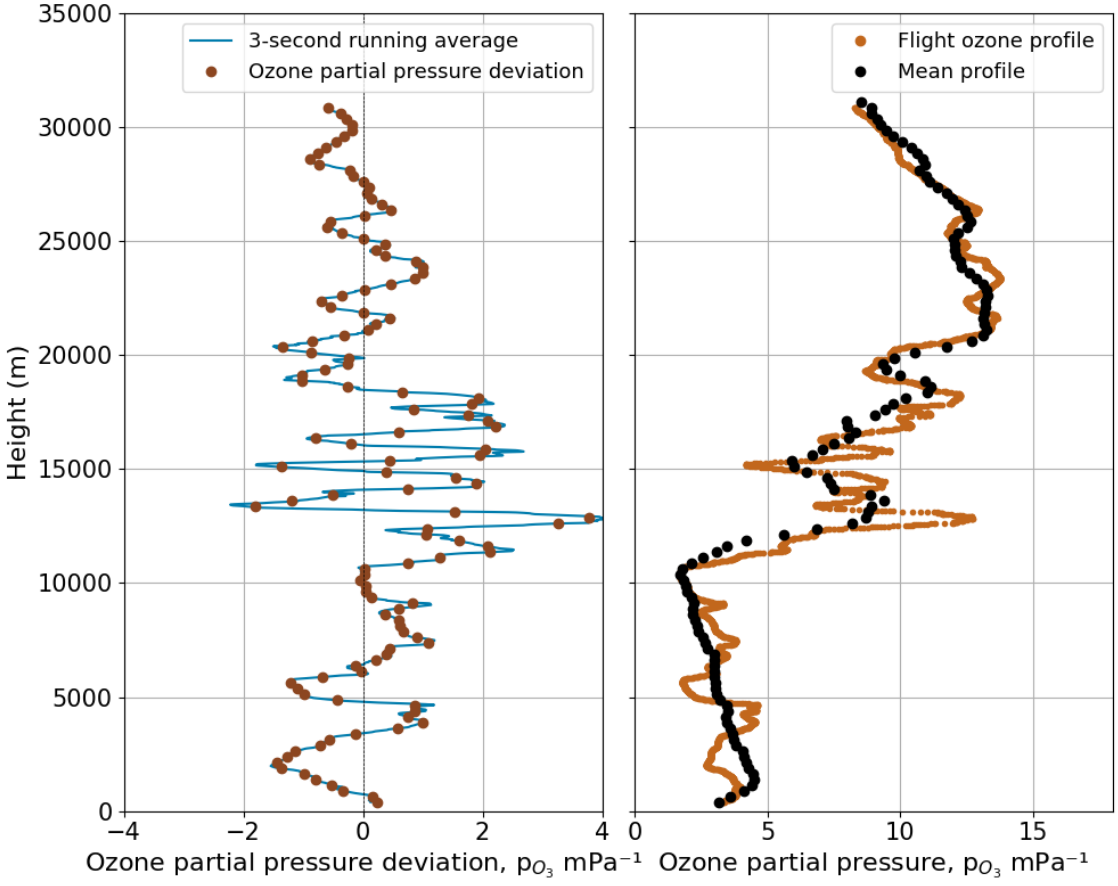

Figure 16. O_3 Vertical profile deviation in ozone partial pressure every 250m. Deviations are relative to a mean June reference profile from all flights, indicated by the vertical black scatter.

is potentially related to overcounting in saturated conditions and requires a specific correction methodology. For the impactors, remaining open during the balloon's descent makes the samples susceptible to contamination from different altitudes. This is a limiting factor in the confidence of the relationship between the particle samples and the air masses from which they originate. Regarding trace gas measurements, the limitations of the CO sensor—primarily its sensitivity to the rapid changes in temperature and pressure experienced during ascent—were evident and constrained its quantitative use.

Future work on the UCASS should focus on developing a correction for potential overcounting, possibly through dedicated laboratory characterizations or by establishing instrument-specific correction factors. For the particle collection system, a critical improvement would be the development and integration of a mechanism to seal the impactors during the descent and landing phases to prevent contamination of the TEM grids. To further enhance the accuracy and reliability of CO measurements, future efforts should focus on refining calibration procedures. Specifically, reducing the uncertainty associated with cross-sensitivities

https://doi.org/10.5194/egusphere-2025-5568
Preprint. Discussion started: 9 December 2025

to other atmospheric gases would significantly improve overall data quality. Alternatively, other types of sensors with greater stability under these conditions should be considered.

In summary, LOONIS represents a valuable and flexible tool for bridging an observational gap in atmospheric science. Its slow ascent provides the high vertical resolution necessary to resolve fine-scale processes, while its cost-effectiveness allows for rapid and targeted deployments to study transient phenomena. The work presented here showcases its ability to deliver an integrated dataset—from real-time microphysics to offline chemical speciation—that is key for improving our process-level understanding of cloud formation and atmospheric transport, and provides a clear path for targeted instrumental improvements.

Code availability. The code for the LOONIS data acquisition and data monitoring software is available from the authors upon request

Data availability. https://doi.org/10.5281/zenodo.17397010

Financial support. Our research was funded by the Deutsche Forschungsgemeinschaft (DFG, German Research Foundation) – TRR 301 – project ID 428312742, in the subproject B02 “BISTUM” within the CRC647 entitled “The Tropopause Region in a Changing Atmosphere” (“TPChange”). We also received financial support from “Dres. Göbel Climate-foundation” Publikationsfonds (OA-Fonds) of TU Darmstadt.

Video supplement. Flight data recording for the payload case study (14 June 2024). This video provides the complete flight telemetry and visual data for the payload case study conducted on 14 June 2024, as discussed in section 4. The file features selectable subtitle tracks that allow for the overlay of synchronized flight data. Viewers can select from the following tracks:

Time Data: Displays synchronized time in yyyy-mm-dd hh:dd:ss format.

Meteorological Data: Displays flight height (m), ambient temperature (Celsius), wind speed (ms^{-1}), and horizontal wind direction.

Combined Data: Displays both time and meteorological data simultaneously.

Author contributions. LV, KK, RW Writing SJ TFS Calibration LK Ozone Calibration, Ozone analyses CvG HR PCB design, technical support MF ESEM sampling AB KS TT POPS calibration HG Backtrajectory calculation, LWC analysis

Competing interests. At least one of the (co-)authors is a member of the editorial board of Atmospheric Measurement Techniques.

https://doi.org/10.5194/egusphere-2025-5568
Preprint. Discussion started: 9 December 2025

References

Abdul-Razzak, H. and Ghan, S. J.: A parameterization of aerosol activation. 1. A parameterization of aerosol activation in the presence of an updraft, Journal of Geophysical Research: Atmospheres, 105, 15 443–15 456, https://doi.org/10.1029/2000JD900045, 2000.

Alphasense: Correcting for Background Currents in Four Electrode Toxic Gas Sensors, Application Note AAN 803-05, Alphasense, Great Notley, Essex, UK, 2019.

Alphasense: Carbon Monoxide sensor CO-B4 Datasheet, Vaisala Oyj, 1st edn., https://ametekcdn.azureedge.net/mediafiles/project/oneweb/oneweb/alphas$b4_datasheet_en_2.pdf?revision:87f7d42e-02c4-4b00-b888-bd9c8d07ed3f$, 2021.

Altstädter, B., Platis, A., Wehner, B., Scholtz, A., Wildmann, N., Hermann, M., Käthner, R., Baars, H., Bange, J., and Lampert, A.: ALADINA – an unmanned research aircraft for observing vertical and horizontal distributions of ultrafine particles within the atmospheric boundary layer, Atmospheric Measurement Techniques, 8, 1627–1639, https://doi.org/10.5194/amt-8-1627-2015, 2015.

Arouca, F. O., Feitosa, N. R., and Coury, J.: Effect of sampling in the evaluation of particle size distribution in nanoaerosols, Powder Technology, 200, 52–59, https://doi.org/10.1016/J.POWTEC.2010.02.007, 2010.

Asher, E., Baron, A., Yu, P., Todt, M., Smale, P., Liley, B., Querel, R., Sakai, T., Morino, I., Jin, Y., Nagai, T., Uchino, O., Hall, E., Cullis, P., Johnson, B., and Thornberry, T. D.: Balloon Baseline Stratospheric Aerosol Profiles (B2SAP)—Perturbations in the Southern Hemisphere, 2019–2022, Journal of Geophysical Research: Atmospheres, 129, e2024JD041 581, https://doi.org/https://doi.org/10.1029/2024JD041581, e2024JD041581 2024JD041581, 2024.

Bates, T. S., Quinn, P. K., Johnson, J. E., Corless, A., Brechtel, F. J., Stalin, S. E., Meinig, C., and Burkhart, J. F.: Measurements of atmospheric aerosol vertical distributions above Svalbard, Norway, using unmanned aerial systems (UAS), Atmospheric Measurement Techniques, 6, 2115–2120, https://doi.org/10.5194/amt-6-2115-2013, 2013.

Baumgardner, D., Avallone, L., Bansemer, A., et al.: In situ measurements of cloud properties, in: Clouds in the Perturbed Climate System: Their Relationship to Energy Balance, Atmospheric Dynamics, and Precipitation, edited by Heintzenberg, J. and Charlson, R. J., pp. 3–21, MIT Press, 2011.

Baumgartner, M., Weigel, R., Achatz, U., Harvey, A., and Spichtinger, P.: Reappraising the appropriate use of a common meteorological quantity: Potential Temperature, https://doi.org/https://doi.org/10.5194/acp-20-15585-2020, 2020.

Birmili, W., Weinhold, K., Rasch, F., Sonntag, A., Sun, J., Merkel, M., Wiedensohler, A., Bastian, S., Schladitz, A., Löschau, G., Cyrys, J., Pitz, M., Gu, J., Kusch, T., Flentje, H., Quass, U., Kaminski, H., Kuhlbusch, T. A. J., Meinhardt, F., Schwerin, A., Bath, O., Ries, L., Gerwig, H., Wirtz, K., and Fiebig, M.: Long-term observations of tropospheric particle number size distributions and equivalent black carbon mass concentrations in the German Ultrafine Aerosol Network (GUAN), Earth System Science Data, 8, 355–382, https://doi.org/10.5194/essd-8-355-2016, 2016.

Bondy, A., Bonanno, D., Moffet, R., Wang, B., Laskin, A., and Ault, A.: The diverse chemical mixing state of aerosol particles in the southeastern United States, Atmospheric Chemistry and Physics, https://doi.org/10.5194/ACP-18-12595-2018, 2018.

Brem, B. and Zhang, Y.: Development of an isokinetic sampler for variable flow velocities., p. 11, https://doi.org/10.13031/2013.25482, 2008.

Carslaw, K. S., Boucher, O., Spracklen, D. V., Mann, G. W., Rae, J. G. L., Woodward, S., and Kulmala, M.: A review of natural aerosol interactions and feedbacks within the Earth system, Atmospheric Chemistry and Physics, 10, 1701–1737, https://doi.org/10.5194/acp-10-1701-2010, 2010.

https://doi.org/10.5194/egusphere-2025-5568
Preprint. Discussion started: 9 December 2025

Chan, K., Schillereff, D. N., Baas, A. C., Chadwick, M. A., Main, B., Mulligan, M., O'Shea, F. T., Pearce, R., Smith, T. E., van Soesbergen, A., Tebbs, E., and Thompson, J.: Low-cost electronic sensors for environmental research: Pitfalls and opportunities, Progress in Physical Geography, 45, 305–338, https://doi.org/10.1177/0309133320956567, 2021.

Costa-Surós, M., Sourdeval, O., Acquistapace, C., Baars, H., Carbajal Henken, C., Genz, C., Hesemann, J., Jimenez, C., König, M., Kretzschmar, J., Madenach, N., Meyer, C. I., Schrödner, R., Seifert, P., Senf, F., Brueck, M., Cioni, G., Engels, J. F., Fieg, K., Gorges, K., Heinze, R., Siligam, P. K., Burkhardt, U., Crewell, S., Hoose, C., Seifert, A., Tegen, I., and Quaas, J.: Detection and attribution of aerosol–cloud interactions in large-domain large-eddy simulations with the ICOsahedral Non-hydrostatic model, Atmospheric Chemistry and Physics, 20, 5657–5678, https://doi.org/10.5194/acp-20-5657-2020, 2020.

Deutscher Wetterdienst: Bodenanalyse 14. Juni 2024 12 UTC, Online; via wetter3.de, https://www.wetter3.de/Archiv/DWD/24061412_DWD_Analyse.gif, accessed on October 9, 2025, 2024.

Dubey, R., Patra, A. K., and Nazneen: Vertical profile of particulate matter: A review of techniques and methods, Air Quality, Atmosphere & Health, 15, 979–1010, 2022.

Dupont, S., Lamaud, E., Irvine, M. R., Bonnefond, J.-M., González-Romero, A., Alastuey, A., González-Flórez, C., Querol, X., Kandler, K., Klose, M., and Pérez García-Pando, C.: Performance of a low-cost optical particle counter (Alphasense OPC-N3) in estimating size-resolved dust emission flux using eddy covariance, Atmospheric Measurement Techniques, 18, 2183–2200, https://doi.org/10.5194/amt-18-2183-2025, 2025.

Ebert, M., Weigel, R., Kandler, K., Günther, G., Molleker, S., Grooß, J.-U., Vogel, B., Weinbruch, S., and Borrmann, S.: Chemical analysis of refractory stratospheric aerosol particles collected within the arctic vortex and inside polar stratospheric clouds, Atmospheric Chemistry and Physics, 16, 8405–8421, https://doi.org/10.5194/acp-16-8405-2016, 2016.

Ebert, M., Weigel, R., Weinbruch, S., Schneider, L., Kandler, K., Lauterbach, S., Köllner, F., Plöger, F., Günther, G., Vogel, B., and Borrmann, S.: Characterization of refractory aerosol particles collected in the tropical upper troposphere–lower stratosphere (UTLS) within the Asian tropopause aerosol layer (ATAL), Atmospheric Chemistry and Physics, 24, 4771–4788, https://doi.org/10.5194/acp-24-4771-2024, 2024.

EN-SCI: ECC Ozonesonde Operation Manual, EN-SCI Corporation, 325 W 121ST AVENUE WESTMINSTER, COLORADO, USA 8023, 1st edn., available at https://www.en-sci.com/wp-content/uploads/2020/02/Ozonesonde-Flight-Preparation-Manual.pdf, 2019.

European Commission: Commission Implementing Regulation (EU) No 923/2012 of 26 September 2012 laying down the common rules of the air and operational provisions regarding services and procedures in air navigation and amending Implementing Regulation (EU) No 1035/2011 and Regulations (EC) No 1265/2007, (EC) No 1794/2006, (EC) No 730/2006, (EC) No 1033/2006 and (EU) No 255/2010, https://eur-lex.europa.eu/legal-content/EN/TXT/PDF/?uri=CELEX:32012R0923&from=DE, cELEX number: 32012R0923, 2012.

Evan, S., Brioude, J., Rosenlof, K., Davis, S., Vömel, H., Héron, D., Posny, F., Metzger, J., Duflot, V., Payen, G., Vérèmes, H., Keckhut, P., and Cammas, J.: Effect of deep convection on the TTL composition over the Southwest Indian Ocean during austral summer, Atmospheric Chemistry and Physics, pp. 1–44, https://doi.org/10.5194/acp-2019-1072, 2020.

Feingold, G., McComiskey, A., Yamaguchi, T., Johnson, J. S., Carslaw, K., and Schmidt, K. S.: New approaches to quantifying aerosol influence on the cloud radiative effect, Proceedings of the National Academy of Sciences, 113, 5812 – 5819, https://doi.org/10.1073/pnas.1514035112, 2016.

Gao, R.-S., Telg, H., McLaughlin, R. J., Ciciora, S. J., Watts, L. A., Richardson, M. S., Schwarz, J. P., Perring, A. E., Thornberry, T. D., Rollins, A. W., Markovic, M. Z., Bates, T. S., Johnson, J. E., and Fahey, D. W.: A light-weight, high-sensitivity particle spectrometer for $PM_{2.5}$ aerosol measurements, Aerosol Science and Technology, 50, 88–99, https://doi.org/10.1080/02786826.2015.1131809, 2016.

https://doi.org/10.5194/egusphere-2025-5568
Preprint. Discussion started: 9 December 2025

Gaston, C. J.: Re-examining Dust Chemical Aging and Its Impacts on Earth's Climate, Accounts of Chemical Research, 53, 1005–1013, https://doi.org/10.1021/acs.accounts.0c00102, pMID: 32349473, 2020.

Girdwood, J.: Optical Measurement of Airborne Particles on Unmanned Aircraft, Ph.D. thesis, University of Hertfordshire Research Archive, https://uhra.herts.ac.uk/handle/2299/27277, 2022.

Girdwood, J., Ballington, H., Stopford, C., Lewis, R., and Hesse, E.: Calibration of optical particle spectrometers using mounted fibres, Atmospheric Measurement Techniques, 18, 305–317, https://doi.org/10.5194/amt-18-305-2025, 2025.

Golden, J. H., Serafin, R., Lally, V., and Facundo, J.: Atmospheric Sounding Systems, pp. 50–70, American Meteorological Society, Boston, MA, ISBN 978-1-935704-20-1, https://doi.org/10.1007/978-1-935704-20-1_4, 1986.

Hagen Telg, Daniel M. Murphy, T. S. B. J. E. J. P. K. Q. F. G. and Gao, R.-S.: A practical set of miniaturized instruments for vertical profiling of aerosol physical properties, Aerosol Science and Technology, 51, 715–723, https://doi.org/10.1080/02786826.2017.1296103, 2017.

Han, P., Mei, H., Liu, D., Zeng, N., Tang, X., Wang, Y., and Pan, Y.: Calibrations of Low-Cost Air Pollution Monitoring Sensors for CO, NO2, O3, and SO2, Sensors, 21, https://doi.org/10.3390/s21010256, 2021.

Hersbach, H., Bell, B., Berrisford, P., Hirahara, S., Horányi, A., Muñoz-Sabater, J., Nicolas, J., Peubey, C., Radu, R., Schepers, D., Simmons, A., Soci, C., Abdalla, S., Abellan, X., Balsamo, G., Bechtold, P., Biavati, G., Bidlot, J., Bonavita, M., De Chiara, G., Dahlgren, P., Dee, D., Diamantakis, M., Dragani, R., Flemming, J., Forbes, R., Fuentes, M., Geer, A., Haimberger, L., Healy, S., Hogan, R. J., Hólm, E., Janisková, M., Keeley, S., Laloyaux, P., Lopez, P., Lupu, C., Radnoti, G., de Rosnay, P., Rozum, I., Vamborg, F., Villaume, S., and Thépaut, J.-N.: The ERA5 global reanalysis, Quarterly Journal of the Royal Meteorological Society, 146, 1999–2049, https://doi.org/https://doi.org/10.1002/qj.3803, 2020.

Heutte, B., Bergner, N., Angot, H., Pernov, J. B., Dada, L., Mirrielees, J. A., Beck, I., Baccarini, A., Boyer, M., Creamean, J. M., Daellenbach, K. R., El Haddad, I., Frey, M. M., Henning, S., Laurila, T., Moschos, V., Petäjä, T., Pratt, K. A., Quéléver, L. L. J., Shupe, M. D., Zieger, P., Jokinen, T., and Schmale, J.: Observations of high-time-resolution and size-resolved aerosol chemical composition and microphysics in the central Arctic: implications for climate-relevant particle properties, Atmospheric Chemistry and Physics, 25, 2207–2241, https://doi.org/10.5194/acp-25-2207-2025, 2025.

Huang, M.: Differences in the Ice Particle Shattering Impact on the CIP Measurements in the Stratiform Cloud Region and the Embedded Convection Region, Water, https://doi.org/10.3390/w13172322, 2021.

Jacobson, M. Z.: Development of mixed-phase clouds from multiple aerosol size distributions and the effect of the clouds on aerosol removal, Journal of Geophysical Research: Atmospheres, 108, https://doi.org/https://doi.org/10.1029/2002JD002691, 2003.

Johnson, R.: Environmental Scanning Electron Microscopy: An Introduction to ESEM, Philips Electron Optics, Eindhoven, The Netherlands, 2nd printing edn., 1996.

Joly, L., Maamary, R., Decarpenterie, T., Cousin, J., Dumelié, N., Chauvin, N., Legain, D., Tzanos, D., and Durry, G.: Atmospheric Measurements by Ultra-Light SpEctrometer (AMULSE) Dedicated to Vertical Profile in Situ Measurements of Carbon Dioxide (CO2) Under Weather Balloons: Instrumental Development and Field Application, Sensors (Basel, Switzerland), 16, https://doi.org/10.3390/s16101609, 2016.

Jost, S., Weigel, R., Kandler, K., Valero, L., Girdwood, J., Stopford, C., Stanley, W., Eichhorn, L. K., von Glahn, C., and Tost, H.: Improving the accuracy in particle concentration measurements of a balloon-borne optical particle counter UCASS, EGUsphere, 2025, 1–29, https://doi.org/10.5194/egusphere-2025-451, 2025.

https://doi.org/10.5194/egusphere-2025-5568
Preprint. Discussion started: 9 December 2025

Kandler, K., Benker, N., Bundke, U., Cuevas, E., Ebert, M., Knippertz, P., Rodríguez, S., Schütz, L., and Weinbruch, S.: Chemical composition and mixing state of ice residuals and aerosol particles in mixed-phase clouds: results from the Cloud and Aerosol Characterization Experiment (CLACE 5), Atmospheric Chemistry and Physics, 7, 5545–5565, https://doi.org/10.5194/acp-7-5545-2007, 2007a.

Kandler, K., Benker, N., Bundke, U., Cuevas, E., Ebert, M., Knippertz, P., Rodríguez, S., Schütz, L., and Weinbruch, S.: Chemical composition and complex refractive index of Saharan Mineral Dust at Izaña, Tenerife (Spain) derived by electron microscopy, Atmospheric Environment, 41, 8058–8074, https://doi.org/https://doi.org/10.1016/j.atmosenv.2007.06.047, 2007b.

Kandler, K., Schütz, L., Deutscher, C., Ebert, M., Hofmann, H., JäCKEL, S., Jaenicke, R., Knippertz, P., Lieke, K., Massling, A., Petzold, A., Schladitz, A., Weinzierl, B., Wiedensohler, A., Zorn, S., and and, S. W.: Size distribution, mass concentration, chemical and mineralogical composition and derived optical parameters of the boundary layer aerosol at Tinfou, Morocco, during SAMUM 2006, Tellus B: Chemical and Physical Meteorology, 61, 32–50, https://doi.org/10.1111/j.1600-0889.2008.00385.x, 2009.

Kandler, K., Hofer, J., Ansmann, A., Althausen, D., Abdullaev, S., Müller, T., Tesche, M., Ebert, M., Weinbruch, S., Schepanski, K., Laurent, B., Ryder, C., Hervo, M., and Leisner, T.: African dust properties and transport from field observations and particle transport modeling: a case study from the CADEX-pol campaign in summer 2015, Atmospheric Chemistry and Physics, 18, 13 985–14 008, https://doi.org/10.5194/acp-18-13985-2018, 2018.

Kasparoglu, S., Meskhidze, N., and Petters, M. D.: Aerosol mixing state, new particle formation, and cloud droplet number concentration in an urban environment, Science of The Total Environment, 951, 175 307, https://doi.org/https://doi.org/10.1016/j.scitotenv.2024.175307, 2024.

Kezoudi, M., Tesche, M., Smith, H. R., Tsekeri, A., Baars, H., Dollner, M., Estellés, V., Bühl, J., Weinzierl, B., Ulanowski, Z., Müller, D., and Amiridis, V.: Measurement report: Balloon-borne in situ profiling of Saharan dust over Cyprus with the UCASS optical particle counter, Atmospheric Chemistry and Physics, 21, 6781–6797, https://doi.org/10.5194/ACP-21-6781-2021, 2021.

Kim, J., Shusterman, A. A., Lieschke, K. J., Newman, C., and Cohen, R. C.: The BErkeley Atmospheric CO_2 Observation Network: field calibration and evaluation of low-cost air quality sensors, Atmospheric Measurement Techniques, 11, 1937–1946, https://doi.org/10.5194/amt-11-1937-2018, 2018.

Kloss, C., Sellitto, P., Renard, J., Baron, A., Bègue, N., Legras, B., Berthet, G., Briaud, E., Carboni, E., Duchamp, C., Duflot, V., Jacquet, P., Marquestaut, N., Metzger, J., Payen, G., Ranaivombola, M., Roberts, T., Siddans, R., and Jégou, F.: Aerosol Characterization of the Stratospheric Plume From the Volcanic Eruption at Hunga Tonga 15 January 2022, Geophysical Research Letters, 49, https://doi.org/10.1029/2022GL099394, 2022.

Koehler, K. A., Kreidenweis, S. M., DeMott, P. J., Petters, M. D., Prenni, A. J., and Carrico, C. M.: Hygroscopicity and cloud droplet activation of mineral dust aerosol, Geophysical Research Letters, 36, https://doi.org/https://doi.org/10.1029/2009GL037348, 2009.

Kunz, M., Abbas, S. S., Bauckholt, M., Böhmländer, A., Feuerle, T., Gasch, P., Glaser, C., Groß, J., Hajnsek, I., Handwerker, J., Hase, F., Khordakova, D., Knippertz, P., Kohler, M., Lange, D., Latt, M., Laube, J., Martin, L., Mauder, M., Möhler, O., Mohr, S., Reitter, R. W., Rettenmeier, A., Rolf, C., Saathoff, H., Schrön, M., Schütze, C., Spahr, S., Späth, F., Vogel, F., Völksch, I., Weber, U., Wieser, A., Wilhelm, J., Zhang, H., and Dietrich, P.: Swabian MOSES 2021: An interdisciplinary field campaign for investigating convective storms and their event chains, Frontiers in Earth Science, Volume 10 - 2022, https://doi.org/10.3389/feart.2022.999593, 2022.

Li, J., Chen, X., Wang, Z., Du, H., Yang, W., Sun, Y., Hu, B., Li, J., Wang, W., Wang, T., Fu, P., and Huang, H.: Radiative and heterogeneous chemical effects of aerosols on ozone and inorganic aerosols over East Asia, Science of The Total Environment, 622-623, 1327–1342, https://doi.org/https://doi.org/10.1016/j.scitotenv.2017.12.041, 2018.

https://doi.org/10.5194/egusphere-2025-5568
Preprint. Discussion started: 9 December 2025

Li, T., Yu, Y., Wang, X., Liu, X., Mao, Q., and Yuan, Y.: A review of aerosol-cloud interactions: Mechanisms, climate effects, and observation methods, Atmospheric Research, 325, 108 267, https://doi.org/https://doi.org/10.1016/j.atmosres.2025.108267, 2025a.

Li, Y., Zhang, C., Su, W., Jiang, S., Nie, D., Wang, Y., Wang, Y., He, H., Chen, Q., Martin, S. T., and Ye, J.: Copter-Type UAV-Based Sensing in Atmospheric Chemistry: Recent Advances, Applications, and Future Perspectives, Environmental Science & Technology, 59, 13 532–13 550, https://doi.org/10.1021/acs.est.5c00074, pMID: 40618262, 2025b.

Liu, Z., Osborne, M., Anderson, K., Shutler, J. D., Wilson, A., Langridge, J., Yim, S. H. L., Coe, H., Babu, S., Satheesh, S. K., Zuidema, P., Huang, T., Cheng, J. C. H., and Haywood, J.: Characterizing the performance of a POPS miniaturized optical particle counter when operated on a quadcopter drone, Atmospheric Measurement Techniques, 14, 6101–6118, https://doi.org/10.5194/amt-14-6101-2021, 2021.

Mamali, D., Marinou, E., Sciare, J., Pikridas, M., Kokkalis, P., Kottas, M., Binietoglou, I., Tsekeri, A., Keleshis, C., Engelmann, R., Baars, H., Ansmann, A., Amiridis, V., Russchenberg, H., and Biskos, G.: Vertical profiles of aerosol mass concentration derived by unmanned airborne in situ and remote sensing instruments during dust events, Atmospheric Measurement Techniques, 11, 2897–2910, https://doi.org/10.5194/amt-11-2897-2018, 2018.

Manisalidis, I., Stavropoulou, E., Stavropoulos, A., and Bezirtzoglou, E.: Environmental and Health Impacts of Air Pollution: A Review, Frontiers in Public Health, 8, https://doi.org/10.3389/fpubh.2020.00014, 2020.

Misumi, R., Uji, Y., Tobo, Y., Miura, K., Uetake, J., Iwamoto, Y., Maesaka, T., and Iwanami, K.: Characteristics of Droplet Size Distributions in Low-Level Stratiform Clouds Observed from Tokyo Skytree, Journal of the Meteorological Society of Japan, 96, 405–413, https://doi.org/10.2151/JMSJ.2018-040, 2018.

Moormann, L., Böttger, T., Schuhmann, P., Valero, L., Fachinger, F., and Drewnick, F.: The Flying Laboratory FLab: development and application of a UAS to measure aerosol particles and trace gases in the lower troposphere, Atmospheric Measurement Techniques, 18, 1441–1459, https://doi.org/10.5194/amt-18-1441-2025, 2025.

Morgan, W., Allan, J., Bower, K., Highwood, E., Liu, D., McMeeking, G., Northway, M., Williams, P., Krejci, R., and Coe, H.: Airborne measurements of the spatial distribution of aerosol chemical composition across Europe and evolution of the organic fraction, Atmospheric Chemistry and Physics, 10, 4065–4083, https://doi.org/10.5194/ACP-10-4065-2010, 2010.

Noh, Y.-J., Seaman, C. J., Haar, T. H. V., and Liu, G.: In Situ Aircraft Measurements of the Vertical Distribution of Liquid and Ice Water Content in Midlatitude Mixed-Phase Clouds, Journal of Applied Meteorology and Climatology, 52, 269 – 279, https://doi.org/10.1175/JAMC-D-11-0202.1, 2013.

O'Sullivan, D., Marenco, F., Ryder, C. L., Pradhan, Y., Kipling, Z., Johnson, B., Benedetti, A., Brooks, M., McGill, M., Yorks, J., and Selmer, P.: Models transport Saharan dust too low in the atmosphere: a comparison of the MetUM and CAMS forecasts with observations, Atmospheric Chemistry and Physics, 20, 12 955–12 982, https://doi.org/10.5194/acp-20-12955-2020, 2020.

Papayannis, A., Amiridis, V., Mona, L., Tsaknakis, G., Balis, D., Bösenberg, J., Chaikovski, A., De Tomasi, F., Grigorov, I., Mattis, I., Mitev, V., Müller, D., Nickovic, S., Pérez, C., Pietruczuk, A., Pisani, G., Ravetta, F., Rizi, V., Sicard, M., Trickl, T., Wiegner, M., Gerding, M., Mamouri, R. E., D'Amico, G., and Pappalardo, G.: Systematic lidar observations of Saharan dust over Europe in the frame of EARLINET (2000–2002), Journal of Geophysical Research: Atmospheres, 113, https://doi.org/https://doi.org/10.1029/2007JD009028, 2008.

Parker Hannifin Corporation: CTS Series Micro Diaphragm Pumps (air/gas) Datasheet, Parker Hannifin Corporation, Precision Fluidics Division, Hollis, NH, https://www.parker.com/content/dam/Parker-com/Literature/Precision-Fluidics/Miniature-Diaphragm-Pumps/CTS-pump-data-sheet.pdf, 2020.

Pikridas, M., Bezantakos, S., Močnik, G., Keleshis, C., Brechtel, F., Stavroulas, I., Demetriades, G., Antoniou, P., Vouterakos, P., Argyrides, M., Liakakou, E., Drinovec, L., Marinou, E., Amiridis, V., Vrekoussis, M., Mihalopoulos, N., and Sciare, J.: On-flight intercomparison

https://doi.org/10.5194/egusphere-2025-5568
Preprint. Discussion started: 9 December 2025

of three miniature aerosol absorption sensors using unmanned aerial systems (UASs), Atmospheric Measurement Techniques, 12, 6425–6447, https://doi.org/10.5194/amt-12-6425-2019, 2019.

Piper, D., Kunz, M., Allen, J., and Mohr, S.: Investigation of the temporal variability of thunderstorms in central and western Europe and the relation to large-scale flow and teleconnection patterns, Quarterly Journal of the Royal Meteorological Society, 145, 3644 – 3666, https://doi.org/10.1002/qj.3647, 2019.

Pöhlker, M., Pöhlker, C., Quaas, J., Mülmenstädt, J., Pozzer, A., Andreae, M., Artaxo, P., Block, K., Coe, H., Ervens, B., Gallimore, P., Gaston, C., Gunthe, S., Henning, S., Herrmann, H., Krüger, O., Mcfiggans, G., Poulain, L., Raj, S., Reyes-Villegas, E., Royer, H., Walter, D., Wang, Y., and Pöschl, U.: Global organic and inorganic aerosol hygroscopicity and its effect on radiative forcing, Nature Communications, 14, 6139, https://doi.org/10.1038/s41467-023-41695-8, 2023.

Pruppacher, H., Klett, J., and Wang, P.: Microphysics of Clouds and Precipitation, Aerosol Science and Technology, 28, 381–382, https://doi.org/10.1080/02786829808965531, 1998.

Pruppacher, H. R. and Klett, J. D.: Microphysics of Clouds and Precipitation, Springer, this is a comprehensive reference detailing all stages of cloud droplet growth, including the collisional processes that produce large droplets (>40 μm) and initiate rain., 2010.

Pöschl, U.: Atmospheric Aerosols: Composition, Transformation, Climate and Health Effects, Angewandte Chemie International Edition, 44, 7520–7540, https://doi.org/10.1002/anie.200501122, 2005.

Pöschl, U., Martin, S. T., Sinha, B., Chen, Q., Gunthe, S. S., Huffman, J. A., Borrmann, S., Farmer, D. K., Garland, R. M., Helas, G., Jimenez, J. L., King, S. M., Manzi, A., Mikhailov, E., Pauliquevis, T., Petters, M. D., Prenni, A. J., Roldin, P., Rose, D., Schneider, J., Su, H., Zorn, S. R., Artaxo, P., and Andreae, M. O.: Rainforest Aerosols as Biogenic Nuclei of Clouds and Precipitation in the Amazon, Science, 329, 1513–1516, https://doi.org/10.1126/science.1191056, 2010.

Rades, S., Hodoroaba, V., Salge, T., Wirth, T., Lobera, M. P., Labrador, R., Natte, K., Behnke, T., Gross, T., and Unger, W.: High-resolution imaging with SEM/T-SEM, EDX and SAM as a combined methodical approach for morphological and elemental analyses of single engineered nanoparticles, RSC Advances, 4, 49 577–49 587, https://doi.org/10.1039/C4RA05092D, 2014.

Rossi, A., Zurria, A., Porpora, D., Rossi, L., Nunzio, C. D., Depaolis, E., Misercola, L., Pasquale, F., Agresti, G., Morichetti, G., Boccacci, G., Valant, E., Marzioli, P., Santoni, F., and Piergentili, F.: Balloon-Borne Software Defined Receiver for GNSS Radio Occultation Measurements: ROMULUS Experiment, 2022 IEEE 9th International Workshop on Metrology for AeroSpace (MetroAeroSpace), pp. 208–212, https://doi.org/10.1109/MetroAeroSpace54187.2022.9855995, 2022.

Schön, M., Savvakis, V., Kezoudi, M., Platis, A., and Bange, J.: OPC-Pod: A New Sensor Payload to Measure Aerosol Particles for Small Uncrewed Aircraft Systems, Journal of Atmospheric and Oceanic Technology, 41, 499 – 513, https://doi.org/10.1175/JTECH-D-23-0078.1, 2024.

Seinfeld, J., Bretherton, C., Carslaw, K., Coe, H., DeMott, P., Dunlea, E., Feingold, G., Ghan, S., Guenther, A., Kahn, R., Kraucunas, I., Kreidenweis, S., Molina, M., Nenes, A., Penner, J., Prather, K., Ramanathan, V., Ramaswamy, V., Rasch, P., Ravishankara, A., Rosenfeld, D., Stephens, G., and Wood, R.: Improving our fundamental understanding of the role of aerosol-cloud interactions in the climate system, Proceedings of the National Academy of Sciences, 113, 5781 – 5790, https://doi.org/10.1073/pnas.1514043113, 2016.

Seinfeld, J. H. and Pandis, S. N.: Atmospheric Chemistry and Physics: From Air Pollution to Climate Change, John Wiley Sons, Hoboken, NJ, 3 edn., 2016.

Sensidyne, LP: Gilian Gilibrator 2 USB Calibration System Operation & Service Manual, St. Petersburg, FL, https://sensidyne.com/wp-content/uploads/2024/03/Gilibrator-2-USB-User-Manual_850190M-rU.pdf, revision U, Document No. 850190M, 2020.

https://doi.org/10.5194/egusphere-2025-5568
Preprint. Discussion started: 9 December 2025

Sigma-Aldrich: Lycopodium (Product No. 19108), https://www.sigmaaldrich.com/specification-sheets/396/372/19108-BULK-F.pdf, accessed on 2025-07-15, 2025a.

Sigma-Aldrich: Glass beads, acid-washed (Product No. 904368), https://www.sigmaaldrich.com/specification-sheets/422/465/904368-BULK_____ALDRICH__.pdf, accessed on 2025-07-15, 2025b.

Sigma-Aldrich: Glass beads, acid-washed (Product No. G4649), https://www.sigmaaldrich.com/specification-sheets/219/440/G4649-BULK_____SIGMA____.pdf, accessed on 2025-07-15, 2025c.

Smit, H. G. J., Poyraz, D., Van Malderen, R., Thompson, A. M., Tarasick, D. W., Stauffer, R. M., Johnson, B. J., and Kollonige, D. E.: New insights from the Jülich Ozone Sonde Intercomparison Experiment: calibration functions traceable to one ozone reference instrument, Atmospheric Measurement Techniques, 17, 73–112, https://doi.org/10.5194/amt-17-73-2024, 2024.

Smith, H. R., Ulanowski, Z., Kaye, P. H., Hirst, E., Stanley, W., Kaye, R., Wieser, A., Stopford, C., Kezoudi, M., Girdwood, J., Greenaway, R., and Mackenzie, R.: The Universal Cloud and Aerosol Sounding System (UCASS): a low-cost miniature optical particle counter for use in dropsonde or balloon-borne sounding systems, Atmospheric Measurement Techniques, 12, 6579–6599, https://doi.org/10.5194/amt-12-6579-2019, 2019.

Spanu, A., Dollner, M., Gasteiger, J., Bui, T., and Weinzierl, B.: Flow-induced errors in airborne in situ measurements of aerosols and clouds, Atmospheric Measurement Techniques, 13, 1963–1987, https://doi.org/10.5194/AMT-13-1963-2020, 2020.

Sprenger, M., Croci Maspoli, M., and Wernli, H.: Tropopause folds and cross-tropopause exchange: A global investigation based upon ECMWF analyses for the time period March 2000 to February 2001, Journal of Geophysical Research: Atmospheres, 108, https://doi.org/https://doi.org/10.1029/2002JD002587, 2003.

Stohl, A., Bonasoni, P., Cristofanelli, P., Collins, W., Feichter, J., Frank, A., Forster, C., Gerasopoulos, E., Gäggeler, H., James, P., Kentarchos, T., Kromp-Kolb, H., Krüger, B., Land, C., Meloen, J., Papayannis, A., Priller, A., Seibert, P., Sprenger, M., Roelofs, G. J., Scheel, H. E., Schnabel, C., Siegmund, P., Tobler, L., Trickl, T., Wernli, H., Wirth, V., Zanis, P., and Zerefos, C.: Stratosphere-troposphere exchange: A review, and what we have learned from STACCATO, Journal of Geophysical Research: Atmospheres, 108, https://doi.org/https://doi.org/10.1029/2002JD002490, 2003.

Stull, R. B.: An Introduction to Boundary Layer Meteorology, vol. 13 of *Atmospheric and Oceanographic Sciences Library*, Springer Netherlands, ISBN 978-90-277-2769-5, 1988.

Swietlicki, E., Hansson, H. C., Hämeri, K., Svenningsson, B., Massling, A., McFiggans, G., McMurry, P. H., Petäjä, T., Tunved, P., Gysel, M., Topping, D., Weingartner, E., Baltensperger, U., Rissler, J., Wiedensohler, A., and Kulmala, M.: Hygroscopic properties of submicrometer atmospheric aerosol particles measured with H-TDMA instruments in various environments—a review, Tellus B: Chemical and Physical Meteorology, https://doi.org/10.1111/j.1600-0889.2008.00350.x, 2008.

Szopa, S., Naik, V., Adhikary, B., Artaxo, P., Berntsen, T., Collins, W., Fuzzi, S., Gallardo, L., Kiendler-Scharr, A., Klimont, Z., Liao, H., Unger, N., and Zanis, P.: Climate Change 2021: The Physical Science Basis. Contribution of Working Group I to the Sixth Assessment Report of the Intergovernmental Panel on Climate Change, p. 817–922, Cambridge University Press, Cambridge, United Kingdom and New York, NY, USA, https://doi.org/10.1017/9781009157896.008, 2021.

Thouret, V., Cammas, J.-P., Sauvage, B., Athier, G., Zbinden, R., Nédélec, P., Simon, P., and Karcher, F.: Tropopause referenced ozone climatology and inter-annual variability (1994–2003) from the MOZAIC programme, Atmospheric Chemistry and Physics, 6, 1033–1051, https://doi.org/10.5194/acp-6-1033-2006, 2006.

https://doi.org/10.5194/egusphere-2025-5568
Preprint. Discussion started: 9 December 2025

Todt, M. A., Asher, E., Hall, E., Cullis, P., Jordan, A., Xiong, K., Hurst, D. F., and Thornberry, T.: Baseline Balloon Stratospheric Aerosol Profiles (B2SAP)—Systematic Measurements of Aerosol Number Density and Size, Journal of Geophysical Research: Atmospheres, 128, e2022JD038 041, https://doi.org/https://doi.org/10.1029/2022JD038041, e2022JD038041 2022JD038041, 2023.

Trickl, T., Vogelmann, H., Ries, L., Scheel, H.-E., and Sprenger, M.: The underestimated role of stratosphere-to-troposphere transport on tropospheric ozone, Atmospheric Chemistry and Physics Discussions, pp. 1–37, https://doi.org/10.5194/acp-2017-1192, 2018.

Vandergrift, G., Dexheimer, D., Zhang, D., Cheng, Z., Lata, N., Rogers, M., Shrivastava, M., Zhang, J., Gaudet, B., Mei, F., and China, S.: Tethered balloon system and High-Resolution Mass Spectrometry Reveal Increased Organonitrates Aloft Compared to the Ground Level, Environmental science technology, 58, https://doi.org/10.1021/acs.est.4c02090, 2024.

Varga, G.: Changing nature of Saharan dust deposition in the Carpathian Basin (Central Europe): 40 years of identified North African dust events (1979-2018)., Environment international, 139, 105 712, https://doi.org/10.1016/j.envint.2020.105712, 2020.

Worobiec, A., Potgieter-Vermaak, S., Brooker, A., Darchuk, L., Stefaniak, E., and Van Grieken, R.: Interfaced SEM/EDX and micro-Raman Spectrometry for characterisation of heterogeneous environmental particles — Fundamental and practical challenges, Microchemical Journal, 94, 65–72, https://doi.org/https://doi.org/10.1016/j.microc.2009.09.003, 2010.

Yang, Y., Zhao, C., Dong, X., Fan, G., Zhou, Y., Wang, Y., Zhao, L., Lv, F., and Yan, F.: Toward understanding the process-level impacts of aerosols on microphysical properties of shallow cumulus cloud using aircraft observations, Atmospheric Research, 221, 27–33, https://doi.org/https://doi.org/10.1016/j.atmosres.2019.01.027, 2019.